



**Modelling the Atmosphere and its Effects on
the Great Barrier Reef and Queensland**

David Burns

Supervisor: Professor Zoran Ristovski

October 2016

A thesis submitted for the degree of Bachelor of Science (Honours)
Queensland University of Technology
School of Chemistry, Physics, and Mechanical Engineering

Statement of Original Authorship

The work contained in this thesis has not been previously submitted to meet requirements for an award at this or any other higher education institution. To the best of my knowledge and belief, this thesis contains no material previously published or written by another person except where due reference is made.

Signature:

Date:

Abstract

Climate change is a global issue whose contributions are varied and complex requiring in depth study. The CLAW hypothesis (Charlson et al., 1987) proposed a feedback mechanism where stress driven marine biota produced Dimethyl sulphide (DMS) that influenced cloud cover through the creation of cloud condensation nuclei (CCN). DMS is produced by phytoplankton but also by coral (Raina et al., 2013). As the climate shifts towards increased temperature, regions like the Great Barrier Reef (GBR) are increasingly losing coral coverage (Hoegh-Guldberg, 1999). Changes in coral coverage will effect the GBR's production of DMS and thus any potential influences on cloud cover (Fischer et al., 2012). Modelling DMS as it is produced, transformed and transported through the atmosphere, in the GBR region, will provide needed insight into the mechanisms surrounding DMS. This modelling process is dependant on accurate regional atmospheric modelling.

Global models are well developed for the relationship between DMS production and cloud coverage, however they contain large uncertainties (Woodhouse et al., 2010). (Cainey et al., 2007) indicates that this is due to regional variability and calls for regionally specific modelling. While Quinn et al. (2011) used global modelling to refute the global negative feedback loop in the CLAW hypothesis, they acknowledged that more regional modelling needs to be done to understand locally contained negative feedback loops. The satellite study performed by Leahy et al. (2013) indicated the importance of including variation from local sources when modelling, particularly in regions where coral bleaching occurs.

This project focusses on regional atmospheric modelling of the GBR using CSIRO's Conformal-Cubic Atmospheric Model (CCAM). The domains centred on the GBR and Queensland coastline were chosen and modelling runs were performed. The output was explored and tested against measurement data obtained from the Bureau of Meteorology (BOM). As this project was tied to an experimental campaign, back trajectory modelling was performed in the Hybrid Single Particle Lagrangian Integrated Trajectory Model (HYSPLIT) to find suitable locations for the experimental

work.

The HYSPLIT modelling showed that the majority of the air arriving along the Queensland coast came from across the GBR. A month, October, was chosen guided partly by the HYSPLIT work. Locations for data collection were also chosen along with a path and stopping points of a ship voyage.

The CCAM data mirrored the HYSPLIT work, showing that the prevailing winds were the trade winds providing GBR sourced air to the coast for the majority of October. The data also indicated a low pressure system moving across the GBR effecting surface temperatures and wind speeds across the GBR. This highlights the importance of regional atmospheric modelling for modelling DMS production by the reef and its flux into the atmosphere.

The atmospheric conditons for the formation of clouds along the Queensland coastline are present in the CCAM model. The air in which these clouds are formed is almost certainly coming from across the GBR. This fullfills some of the requirements for the GBR influencing rainfall over the eastern part of Queensland.

A comparison between BOM measurement data and the CCAM data was performed. The results showed an underestimation by CCAM of the range of temperatures experienced at the BOM stations. The maximum wind speed was also underestimated by CCAM. These results have been forwarded to the team working on the CCAM model.

Acknowledgements

I would like to thank everyone who has contributed their time and knowledge to help me in completing my research and this thesis.

For their unending and unquestioning support in this journey, along with their help in editing this thesis, I would like to thank my parents and my girlfriend. Perhaps I will finally learn which its is which.

To my good friends and colleagues Joel Alroe and Nassib Jabbour, I thank you so much for your friendship throughout my entire undergraduate experience. Your enthusiasm for science and life in general is infectious.

I would also like to thank the faculty at QUT. In particular my supervisor Zoran Ristovski for giving me the chance to work on this project. And to Konstantin Momot, your support and guidance meant more to me than I can express.

To Markus Thatcher and Martin Cope at CSIRO, thank you for your patient instruction, and for opening up your models and supercomputers to me.

Finally, to every Lecturer and Tutor I came across in my undergraduate classes, you made me who I am, and this thesis possible. Thank you.

Contents

Abstract	v
Acknowledgements	vii
Contents	ix
Chemicals	xiii
Abbreviations	xv
1 Introduction	1
1.1 Research Topic	1
1.2 Research Gap	3
I Literature Review	5
2 Atmosphere	7
2.1 Atmospheric Regions	7
2.1.1 Troposphere	7
2.2 Relative Humidity and Supersaturation	9
2.3 Albedo	10
2.4 Aerosols	10
2.4.1 Particle Formation	11
2.4.2 CCN	12
2.4.3 Köhler Theory	13
3 Dimethyl Sulphide	15
3.1 Chemistry	15
3.1.1 Multiphase Chemistry	17
3.2 Dimethyl Sulphide, Aerosols and the Environment	17
3.2.1 The CLAW Hypothesis	17

CONTENTS

3.2.2	Post-CLAW Research	19
4	The Great Barrier Reef	23
4.1	Coral DMS Production	23
4.2	GBR DMS Production	25
5	Modelling	27
5.1	Back Trajectory Modelling	27
5.2	CCAM, CTM, GLOMAP	28
6	DMS Climatology Modelling	31
6.1	Modelling DMS production	31
6.2	DMS Surface Flux	32
II	Research	35
7	Methodology	37
7.1	Models	37
7.1.1	HYSPLIT	37
7.1.2	CCAM	39
7.1.3	CTM	41
7.1.4	GLOMAP and GLOMAP-mode	42
7.2	Study Design	43
7.2.1	Assessing Locations	43
7.2.2	CCAM and CTM Domains	44
7.2.3	Running the Models	48
7.2.4	Comparison Data	48
7.2.5	CCAM Data Reduction	50
8	Results	53
8.1	HYSPLIT Output	53
8.1.1	Year Long Back Trajectory Histograms	53
8.1.2	Coastal Location Back Trajectory Histograms for October	56
8.1.3	Ship Location Back Trajectory Histograms for October	58
8.2	CCAM Validation	59
8.2.1	Mean Residuals	59
8.2.2	Comparison of BOM and CCAM Data	60
8.3	CCAM Output	62
8.3.1	Surface and Pressure Level Heights	62
8.3.2	Air and Surface Temperatures	63

CONTENTS

8.3.3	Wind Directions and Speed	65
8.3.4	Clouds, Rain and Radiation	66
9	Analysis and Discussion	69
9.1	HYSPLIT Modelling	69
9.1.1	Assessing Locations and Months	69
9.1.2	Advising the Experimental Campaign	69
9.2	CCAM Modelling	71
9.2.1	Modelling of Meteorology Processes	71
9.2.2	Influences on DMS Production	73
9.2.3	Limitations and Reliability of CCAM Data	74
10	Conclusion	77
10.1	Future Research	77
10.2	Closing Remarks	77
	Bibliography	81

CONTENTS

Chemicals

DMS Dimethyl sulfide.

DMSO Dimethyl sulfoxide.

DMSO₂ Dimethyl sulfone.

DMSP Dimethylsulfoniopropionate.

H⁺ Hydrogen.

H₂O Water.

H₂SO₄ Sulfuric acid.

MSA Methane sulfonic acid.

MSIA Methane sulphinic acid.

NO₃ Nitrate.

OH Hydroxide.

SO₂ Sulfur dioxide.

(NH₄)₂SO₄ Ammonium sulphate.

Chemicals

Abbreviations

BOM Bureau of Meteorology.

CCAM The Conformal-Cubic Amtospheric Model.

CCN Cloud Condensation Nuclei.

CLAW The Charlson Lovelock Andreae Warren hypothesis.

CSIRO Commonwealth Scientific and Industrial Research Organisation.

CTM The Chemical Transport Model.

FT Free Troposphere.

GBR Great Barrier Reef.

GCM Global Climate Model.

GLOMAP The GLObal Model of Aerosol Processes.

GLOMAP-mode The mode seperated version of GLOMAP.

HYSPLIT The HYbrid Single Particle Lagrangian Integrated Trajectory model.

MBL Marine Boundary Layer.

MPD Mean Percentage Difference.

NSS Non-Sea-Salt.

PASE Pacific Atmospheric Sulfur Experiment.

PBL Planetary Boundary Layer.

Abbreviations

QLD Queensland.

RCM Regional Climate Model.

RH Relative Humidity.

SST Sea Surface Temperature.

TAPM The Air Pollution Model.

UKCA United Kingdom Chemistry & Aerosols model.

1. Introduction

1.1 Research Topic

Climate change is a global issue effecting every country on Earth. The contributions to climate change are varied and complex requiring in depth study to provide as precise a picture as possible. Changes in the Earth's energy balance result from radiative forcing. Radiative forcing is changes in the amount of radiative energy absorbed or reflected by the ground and atmosphere. The radiative forcing component that currently has the largest uncertainty is aerosols (see figure 1.1) (IPCC, 2015). Aerosols are particles suspended in the air that can directly scatter or absorb radiation, or cause water vapour to condense onto them, acting as cloud condensation nuclei (CCN). Clouds formed from CCN reflect radiation back into space. As such the exploration of aerosols as a radiative forcing mechanism is a key area in understanding the larger issue of climate change.

A major cause of these uncertainties is the necessity for regionally specific aerosol knowledge (IPCC, 2015). Aerosol composition and concentration differs greatly with changes in sources and atmospheric conditions. This regional variation translates to variation in direct scattering/absorption and cloud producing potential, leading to both local and global effects on climate. Thus it is important to develop tested, regionally specific models that take into account these variations (Cainey et al., 2007; Simpson et al., 2014).

In 1987 the CLAW hypothesis was defined in the seminal paper ‘Oceanic phytoplankton, atmospheric sulphur, cloud Albedo and climate’. The abbreviation CLAW was taken from the initials of that paper’s authors, Robert Charlson, James Lovelock, Meinrat Andreae and Stephen Warren. They proposed a feedback mechanism where stress driven marine biota produced chemicals that influenced cloud cover (Charlson et al., 1987). This paper generated a vast body of research involving many scientific disciplines. Dimethyl sulphide (DMS) is the core chemical responsible for the mechanism and is produced by phytoplankton, and as discovered more recently,

1.1. RESEARCH TOPIC

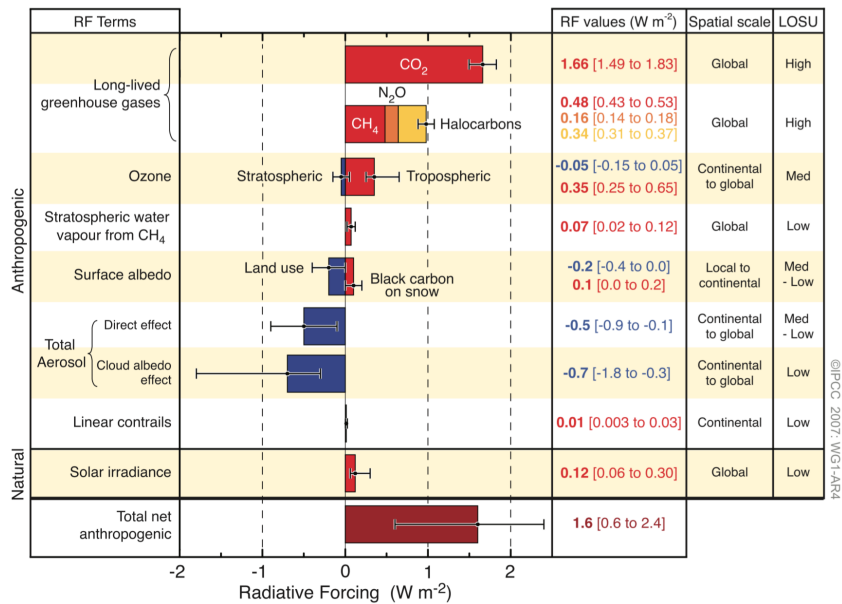


Figure 1.1: A diagram illustrating the various influences on radiative forcing along with their associated uncertainties. From the 2015 Intergovernmental Panel on Climate Change. The largest contributor to uncertainty is currently aerosols (IPCC, 2015).

coral (Raina et al., 2013). As the climate shifts towards increased temperature, regions like the Great Barrier Reef (GBR) are increasingly losing coral coverage (Hoegh-Guldberg, 1999). It is therefore important to examine the potential effects on climate caused by DMS producing biota undergoing climate related reduction.

Initially, it is necessary to understand the role of the atmosphere and its constituents, and where aerosols and DMS are positioned within it. The pathways DMS proceeds down to form CCN involve complicated chemistry (Barnes et al., 2006) and must be explored to ensure the modelling mirrors current theory. The unique climatology of the GBR, including the mechanism and scale with which coral contributes to DMS, needs to be established to provide localised inputs for the group of models. Modelling and the models themselves must be understood to ensure they are being applied correctly and to determine if they are sufficient for simulating the DMS to CCN pathway. Finally, researching the method through which DMS enters the atmosphere, along with previous DMS to CCN modelling attempts, provides insight into the modelling process and what areas of this research area remain unexplored.

Modelling DMS as it is produced, transformed and transported through the atmosphere, in the GBR region, will provide needed insight into the mechanisms surrounding DMS. To do so requires a group of models simulating the different layers of the problem. The bottom most layer is CSIRO's Conformal-Cubic At-

mospheric Model (CCAM) which provides information such as wind speed and temperature (McGregor, 2005). The middle layer is CSIRO's Chemical Transport Model (CTM) which tracks chemical concentrations (Cope et al., 2009). The final layer is the Global Model of Aerosol Processes (GLOMAP) which simulates aerosol interactions and produces aerosol concentrations.

This project takes the first steps in applying this trio of models, with a focus on the regional meteorological model CCAM. The domains centred on the GBR and Queensland coastline were chosen and modelling runs were performed. The output was explored and tested against measurement data obtained from the Bureau of Meteorology (BOM), to establish the efficacy of the model. As this project was tied to an experimental campaign, back trajectory modelling was performed in the Hybrid Single Particle Lagrangian Integrated Trajectory Model (HYSPPLIT) to find suitable locations for the experimental work.

1.2 Research Gap

As the GBR is such a large structure, and ocean temperatures are increasing (Hoegh-Guldberg, 1999), the effect these changes have on coral is critical. The production of DMS by coral is well established (G. B. Jones et al., 2005; Fischer et al., 2012) and changes in coral coverage will effect this production. Furthermore, results from Fischer et al. (2012) indicate that while coral production of DMSP increases in bleaching scenarios, the atmospheric DMS levels decrease drastically. Fischer et al. (2012) suggests this will decrease cloud cover due to the DMS, CCN connection, further driving bleaching. The scale of current coral bleaching levels in the GBR, increases the importance of exploring this relationship.

Global models are well developed for the relationship between DMS production and cloud coverage, however they contain large uncertainties (Woodhouse et al., 2010). Cainey et al. (2007) indicates that this is due to regional variability and calls for regionally specific modelling. While Quinn et al. (2011) used global modelling to refute the global negative feedback loop in the CLAW hypothesis, they acknowledged that more regional modelling needs to be done to understand locally contained negative feedback loops. The satellite study performed by Leahy et al. (2013) indicated the importance of including variation from local sources when modelling, particularly in regions where coral bleaching occurs.

It is clear that regionally specific atmospheric and aerosol models are necessary for reducing uncertainties in climate modelling, and that DMS producing biota serve

1.2. RESEARCH GAP

a role in effecting climate. The GBR is very high producer of DMS (G. B. Jones et al., 2005), with localised influences on production levels, making it an excellent candidate for regional modelling.

Part I

Literature Review

2. Atmosphere

2.1 Atmospheric Regions

The Earth's atmosphere is split into a number of different layers. The factor governing their division is the sign of the change in temperature with respect to altitude. For example, in figure 2.2, a decrease in temperature (T) with an increase in altitude (z) in the troposphere occurs up until the tropopause. The difference in temperature gradients between the different levels of the atmosphere prevent mixing from occurring between layers. This occurs as in most circumstances a parcel of air will rise if $\frac{dT}{dz} < 0$ and fall if $\frac{dT}{dz} > 0$.

2.1.1 Troposphere

The troposphere is the lowest level of the atmosphere sitting between 10 – 15 km above the surface of the Earth. It ends at the tropopause, the first region of constant temperature. The range of altitudes is dependant on time and latitude with the highest region being over the equator, shifting up and down the Earth with its axial tilt (Seinfeld et al., 2012, Chapter 1).

The troposphere is an important region as it contains the majority of the atmosphere's mass (approximately 80 %) and all of its weather. It also contains the highest quantity of water, despite being the smallest region. The layer immediately above the surface of the Earth is called the planetary boundary layer (PBL), or marine boundary layer (MBL) over the ocean (Seinfeld et al., 2012, Chapter 1). The PBL varies greatly in height depending on the surface of the Earth it is over, for example, above the Sahara it can be up to 6 km, while over tropical oceans it is only 100 m (Laing et al., 2011, Chapter 1).

There is a short inversion layer in the troposphere that separates the boundary layer and the free troposphere (FT) (see figure 2.2). It occurs at only a few hundred metres

2.1. ATMOSPHERIC REGIONS

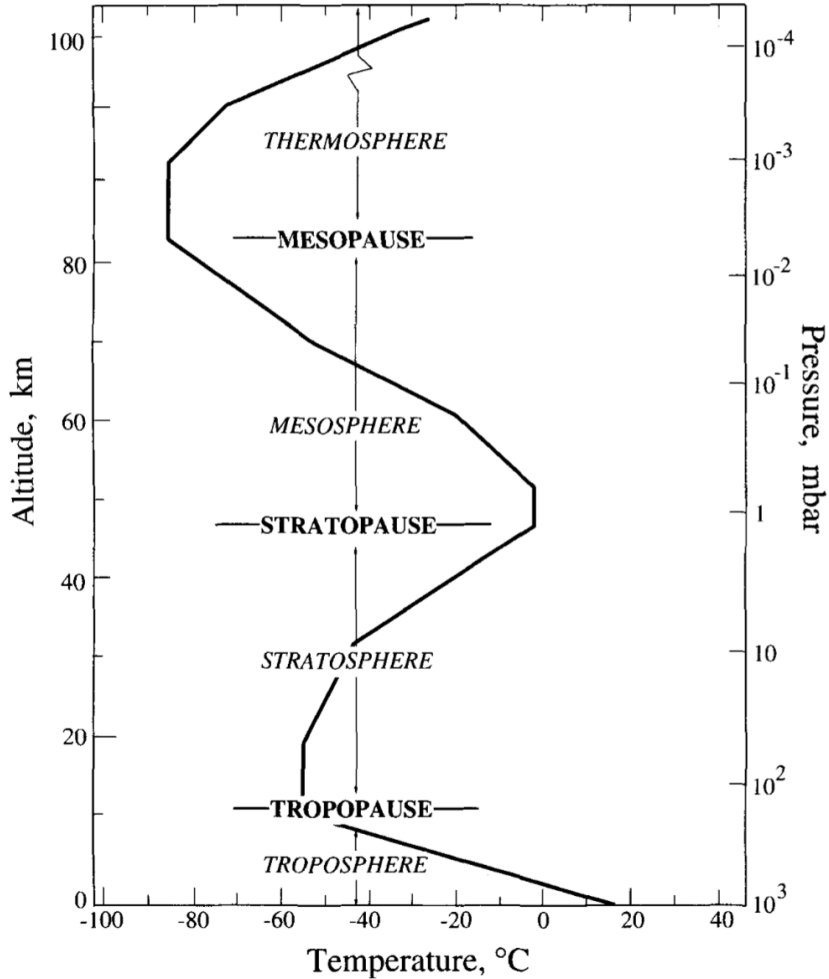


Figure 2.1: The layers of Earth’s atmosphere, separated by pauses in temperature change with respect to altitude (Seinfeld et al., 2012, p. 7)

above tropical oceans (Laing et al., 2011). The FT is relatively free of aerosols, as the inversion layer prevents mixing with the boundary layer. Thus there is a low aerosol surface area greatly decreasing heterogeneous nucleation. The inversion layer is not always present, and clouds can breach this layer permitting chemicals access into the FT from the boundary layer. These conditions promote homogeneous nucleation, which is the formation of new particles (Seinfeld et al., 2012, Chapter 8).

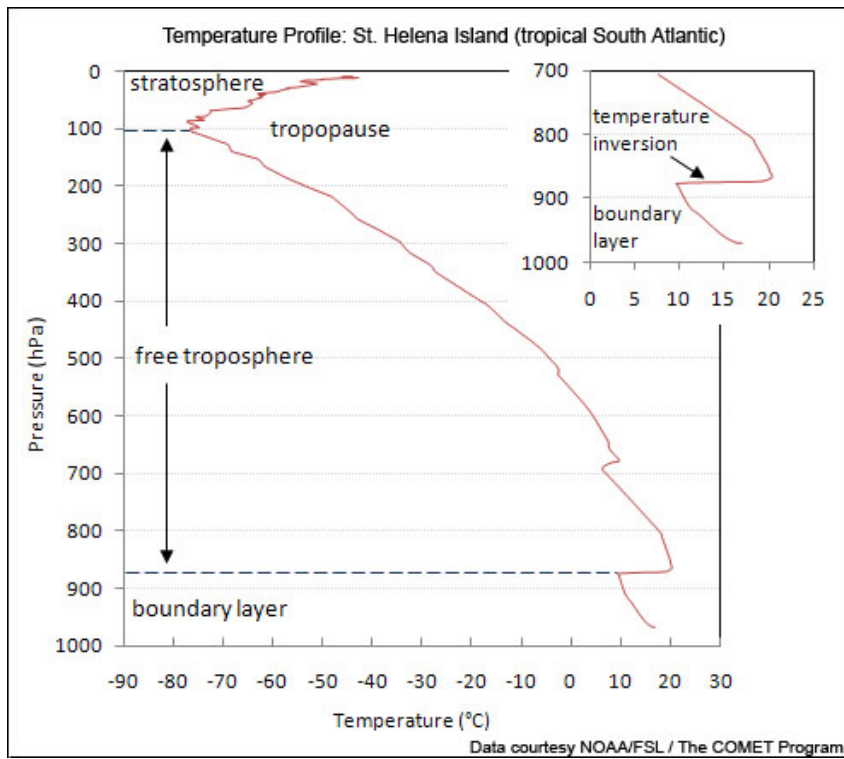


Figure 2.2: An example of the separation between PBL and FT at St. Helena Island. There is an inversion layer present distinguishing the two, however, this obvious separation is not always the case. (Laing et al., 2011, Section 1.5.1)

2.2 Relative Humidity and Supersaturation

The amount of water present in air is usually measured via the relative humidity (RH). RH is the fraction of the partial pressure of the gas phase water $p_{\text{H}_2\text{O}}$ and the saturation vapour pressure for the temperature of the air $p_{\text{H}_2\text{O}}^0$, which is the point at which water condenses (Seinfeld et al., 2012, Chapter 1). Supersaturation occurs when there is a RH greater than 100 % (Rogers et al., 1989).

$$\text{RH} = 100 \times \frac{p_{\text{H}_2\text{O}}}{p_{\text{H}_2\text{O}}^0}. \quad (2.1)$$

When a parcel of moist air rises in the troposphere the temperature within it decreases which increases the RH and a supersaturation can be achieved (Seinfeld et al., 2012, Chapter 1). The temperature decreases due to adiabatic expansion. When this occurs water undergoes spontaneous nucleation onto aerosol particles. A seed particle is required for droplet formation to occur; as homogeneous nucleation

2.3. ALBEDO

of water would require a supersaturation far higher than that seen in the atmosphere. CCN are the aerosol seeds that droplets form around (see section 2.4.2). There is therefore a dependence on the level of supersaturation for an aerosol to act as a CCN, which is generally 0.5 – 2 % (Rogers et al., 1989, Chapter 6).

2.3 Albedo

The albedo of the Earth is given as the ratio between reflected radiation and incident radiation. The amount of light that is not reflected back into space from the surface of the Earth must be absorbed and thus increases the Earth’s temperature. Light may be emitted in the infra-red regime as black-body radiation, which either escapes out into space or is absorbed by greenhouse gases in the atmosphere (Lashof et al., 1990). Water acts as a greenhouse gas, but also acts to increase the albedo of the Earth when formed into clouds. A phenomena that alters the amount of light being absorbed by the Earth is said to exhibit radiative forcing (IPCC, 2015). Aerosols may cause radiative forcing by either directly reflecting or absorbing light, or by assisting in the formation of clouds (Seinfeld et al., 2012, Chapter 4).

2.4 Aerosols

An aerosol is any solid or liquid particle suspended in a gas. In the troposphere there is an abundance of aerosols present, with a vast range of sizes and composition.

Aerosols are generally subdivided into modes that indicate their production mechanism. When plotting a property of a large number of particles, such as their number or surface area, against the log of the aerosol diameter, peaks appear at different diameters, which are called modes (Seinfeld et al., 2012, Chapter 8). The modes are nucleation, Aitken, accumulation, and coarse. The diameters over which these modes are generally found in the atmosphere can be seen in figure 2.3.

There are many properties of aerosols that can be examined, such as volume, surface area, mass, chemical composition, hygroscopicity, and concentration. For cloud formation the most important characteristics are hygroscopicity, a measure of the particles ability to absorb water, and particle diameter, which governs whether a particle is large enough to act as a CCN (Rogers et al., 1989, Chapter 6). The number, or concentration, of aerosols is important for cloud formation to an extent. If too many CCN are present the water vapour concentration may not be high enough to form large droplets (Seinfeld et al., 2012, Chapter 22).

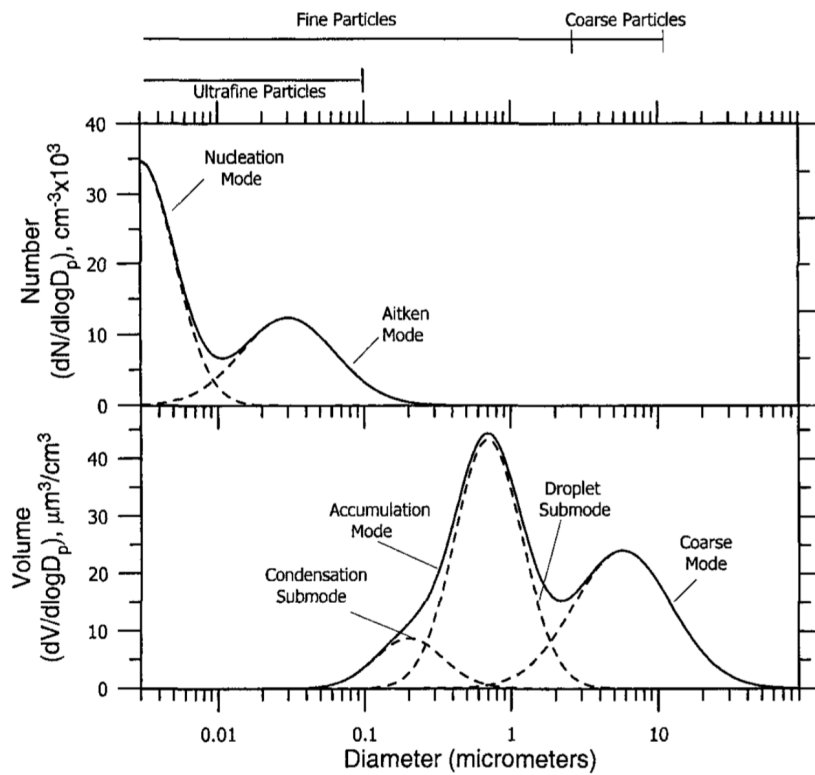


Figure 2.3: An example of the Number and Volume distributions of atmospheric particles indicating the various modes. (Seinfeld et al., 2012, Chapter 8)

The processes that an aerosol undergoes in the atmosphere dictate some of the modes that appear. The nucleation mode arises from particles homogeneously nucleating from a gas, such as sulphuric acid. The accumulation mode is constructed from particles that have condensed vapour such as water, and/or have grown via coagulation, which occurs when multiple aerosol particles stick together. The majority of the accumulation mode peak measured in the atmosphere comes from droplet formation in clouds (Seinfeld et al., 2012, Chapter 8). This droplet sub-mode can be seen in figure 2.3.

2.4.1 Particle Formation

There are two types of aerosols, primary and secondary. The distinction is based on their method of formation.

Primary aerosols are particles that enter the atmosphere directly. In the MBL sea salt particles are an example of primary aerosols (Quinn et al., 2011).

Secondary aerosols are aerosols that have formed in the atmosphere via homogeneous

2.4. AEROSOLS

nucleation. They begin as gases present in high concentrations, in regions with low concentrations of particles, as heterogeneous nucleation is energetically favourable. Creation of secondary particles are dubbed nucleation events, as the atmospheric conditions required for homogeneous nucleation to proceed are uncommon (Seinfeld et al., 2012, Chapter 11).

Because nucleation events are rare and localised in time and space they are difficult to simulate, so the percentage of secondary particles on a global scale has a large uncertainty (IPCC, 2015). Merikanto et al. (2009) modelled global CCN production using the GLOMAP model and showed that between 31 % and 49 % of CCN are secondary particles. Approximately 35 % of these secondary particles were formed in the free and upper troposphere and entrained down into the MBL (Merikanto et al., 2009).

2.4.2 CCN

CCN are aerosols that are able to act as sites for the heterogeneous nucleation of water. The water droplets continue to grow by precipitating gas phase H₂O and eventually become massive enough that they fall out of the sky as rain. The formation of clouds requires CCN, as the atmospheric conditions for homogeneous nucleation of water are never reached. So CCN act as sites for the heterogeneous nucleation of water, forming cloud droplets (Seinfeld et al., 2012, Chapter 17).

CCN are defined for particular supersaturations. This is because whether an aerosol (with a given composition) can act as a CCN, is dependant on the supersaturation of the air it is in. The chemical composition of the particle, or it's hygroscopicity, also affect its ability to act as a CCN. As this information is not always known, empirical equations are often used to describe the concentration of CCN. Take the following equation,

$$\text{CCN}(s) = cs^k. \quad (2.2)$$

Here the concentration of CCN is given as a power function of supersaturation s , where c and k are empirical parameters that conceal the size and composition dependence of CCN. The empirical parameters are sampled locationally with c varying between 25 – 3500 cm⁻³ and k varying between 0.3 – 1.4 (Seinfeld et al., 2012, Chapter 17). If size distributions, composition and supersaturation are known, then Köhler theory (see section 2.4.3) predicts which aerosols may act as CCN (Rissman et al., 2006).

Sources and Sinks for CCN

There are a number of CCN sources. Sea salt is an excellent CCN due to its high hygroscopicity (Randles et al., 2004). It is also abundant in atmospheric regions above the ocean and coastline. It is aerosolised by bubble bursting and wind shear at the surface of the ocean.

Chemicals produced by living organisms can pass through a series of chemical reactions and a subsequent nucleation event to produce CCN. An example of this is DMS produced by phytoplankton, which is further explored in chapter 3. An alternative to DMS derived organic aerosols is dissolved organic matter from dying biota collected at the surface that is aerosolised through bubble bursting (Bigg, 2007).

There are also a number of anthropogenic sources of CCN, however, in the Great Barrier Reef region, only sources from shipping exhaust are likely to be of consequence (Fischer et al., 2012).

Aerosols are readily removed from the atmosphere by rainfall and this is even more apparent for CCN as they provide the site of droplet formation. Rain also collects aerosols as the droplets fall (Rogers et al., 1989). Deposition onto other aerosol particles is another way in which CCN may be removed while it is also possible for aerosols to deposit directly onto the surface of the Earth (Seinfeld et al., 2012, Chapter 9).

2.4.3 Köhler Theory

Köhler theory was first described in a paper written by the theory's namesake Hilding Köhler (Köhler, 1936). It provides a model for the growth of existing particles by heterogeneous nucleation. There are two forces influencing this behaviour, the attraction of a molecule's neighbours (the Kelvin effect), and the concentration of the solution (the solute effect) (Rogers et al., 1989).

For a particle of diameter D_p , the log of the ratio between the water vapour pressure of a droplet and a flat surface is given as a function of the molecular mass of water M_w , the surface tension σ_w , the gas constant R , the temperature T , the water density ρ_w , and the number of moles of the solute n_s .

$$\ln \left(\frac{p_w(D_p)}{p^\circ} \right) = \frac{4M_w\sigma_w}{RT\rho_w D_p} - \frac{6n_s M_w}{\pi \rho_w D_p^3}. \quad (2.3)$$

2.4. AEROSOLS

Substituting in the known constants produces $\frac{4M_w\sigma_w}{RT\rho_w} \approx \frac{0.66}{T}$ and $\frac{6n_s M_w}{\pi \rho_w} \approx \frac{3.44 \times 10^{13} v m_s}{M_s}$ with units μm (Seinfeld et al., 2012, p. 770). The moles of solute n_s is given by the ratio between the number of ions per molecule v , the solute particle mass m_s and the solute molar mass M_s . Substituting into equation (2.3) gives,

$$\frac{p_w(D_p)}{p^\circ} = e^{\frac{0.66}{T D_p}} e^{-\frac{3.44 \times 10^{13} v m_s}{M_s D_p^3}}. \quad (2.4)$$

Here the first exponential term represents the Kelvin effect and the second represents the solute effect.

Plotting equation (2.4) produces Köhler curves that show, for an initial dry particle size, the required supersaturation for particle growth to occur even as the particle itself grows and changes concentration. An example of Köhler curves for different seed diameters of ammonium sulphate $(\text{NH}_4)_2\text{SO}_4$ can be seen in figure 2.4. Here, equation (2.4) has been plotted with $v = 3$, $M_s = 132.14 \text{ g mol}^{-1}$.

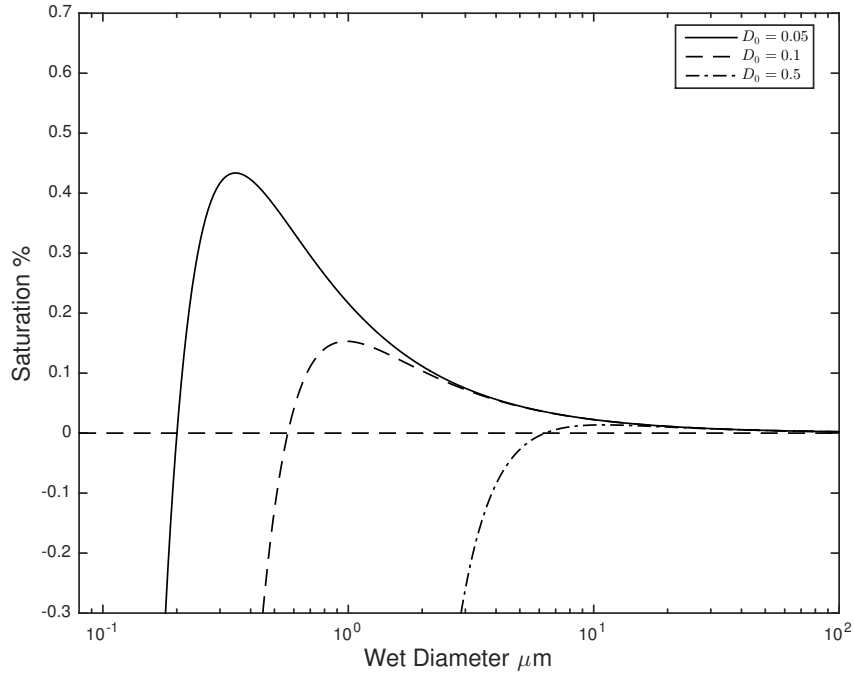


Figure 2.4: The Köhler curves for ammonium sulphate $(\text{NH}_4)_2\text{SO}_4$ for three dry diameters $0.05, 0.1, 0.5 \mu\text{m}$ using approximations from Seinfeld et al. (2012, p. 770)

There are a number of variations to the general form of the Köhler curve equation that deal with alternate conditions, such as insoluble seed particles, and mixes of soluble and insoluble seeds (Seinfeld et al., 2012, Chapter 17).

3. Dimethyl Sulphide

Dimethyl sulphide (DMS) is a naturally produced chemical that has been theorised to influence cloud coverage and potentially act as a negative feedback mechanism for climate change (Charlson et al., 1987). DMS enters the atmosphere and goes through an array of chemical reactions to produce sulphuric acid (H_2SO_4) (Barnes et al., 2006), which may then nucleate into aerosols that can act as CCN. Measurements of aerosols in the atmosphere, particular remote marine areas show a large percentage being of the non-sea salt sulphate variety, potentially sourced from DMS (O'Dowd et al., 1997).

3.1 Chemistry

The chemical processes that DMS and dimethyl sulfoxide DMSO undergo in the atmosphere are extremely complicated with many competing pathways (see figure 3.2). Barnes et al. (2006) have reviewed the extensive literature on this subject, with great detail. They split the problem into three sections, the first, DMS reactions and products, the second, DMSO reactions and products, and the third, multiphase chemistry of the DMS pathways.

The reaction processes for DMS are reactions with the OH radical, the NO_3 radical, and with Halogen Atoms and Oxides. During the day the dominant reaction is the addition pathway through OH, while at night it is the abstraction pathway through NO_3 as seen in figure 3.2 (Barnes et al., 2006). Pathways involving halogen species are generally ignored in modelling due to low availability, though levels of hypobromite high enough to be influential have been measured in the troposphere (Platt et al., 2003).

DMSO appears to be the major product of DMS oxidation in the atmosphere. Its reactions are the same as for DMS listed above. The atmospheric lifetimes calculated indicate that OH radicals dominate reactions for DMSO (Barnes et al.,

3.1. CHEMISTRY

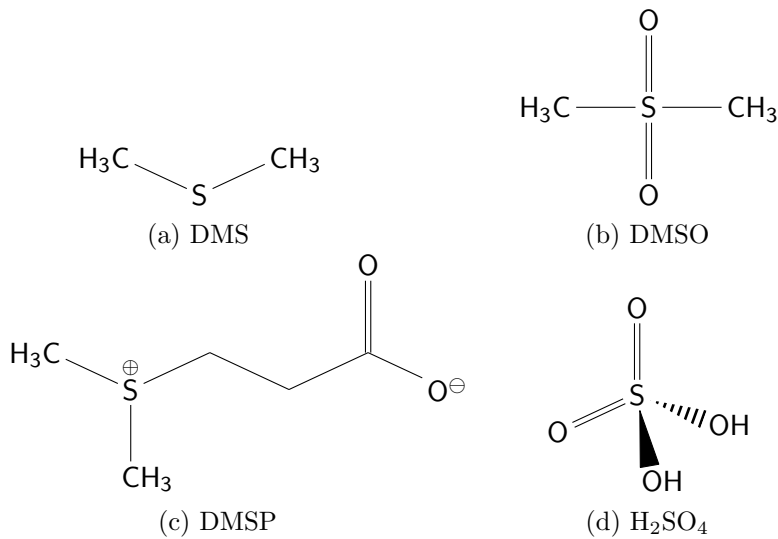


Figure 3.1: The chemical structure of important chemicals relating to DMS

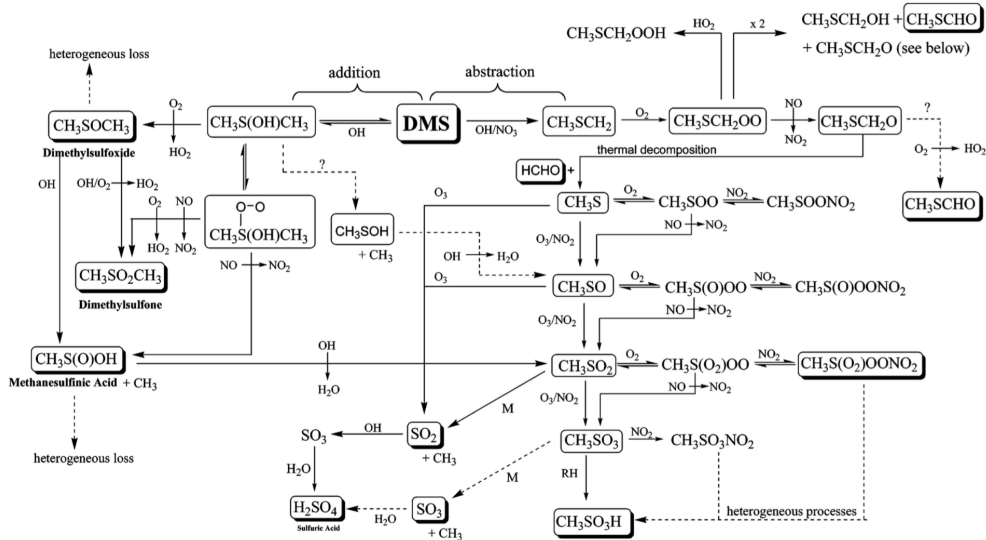


Figure 3.2: The reaction scheme for DMS oxidised by NO_3 and OH radicals (Barnes et al., 2006).

2006). Methane sulphinic acid (MSIA) is a product of this reaction, which goes on to form methane sulphonic acid (MSA). DMSO₂ is also a product of this reaction and was considered the most prevalent pathway, but Barnes et al. (2006) found instead that the MSIA pathway heavily dominates. SO₂ is the largest possible outcome of MSA oxidation.

3.1.1 Multiphase Chemistry

The pathways examined in the preceding section are for gas phase reactions. However the atmosphere also contains liquid water in the form of droplets leading to aqueous phase reactions. The difference between gas and aqueous phase reactions is largely due to the availability of H_2O and H^+ (Barnes et al., 2006). A combination of the two, multiphase chemistry, is needed. Interestingly, DMS is not as soluble in water as DMSO, DMSO_2 , MSA and MSIA so its multiphase reactions are not as important.

Barnes et al. (2006) have analysed the multiphase chemistry of all five chemicals and recommend that modellers implement the multiphase chemistry they have illustrated. They include a list of aqueous phase rate coefficients for the five chemicals of major interest, though do not consider a coupling of the gas and aqueous-phase systems necessary. Jacob (2000) provides a method for calculating chemical uptake by aerosols, while Henry's law is recommended for calculating concentrations, as an approximation.

3.2 Dimethyl Sulphide, Aerosols and the Environment

3.2.1 The CLAW Hypothesis

In the CLAW hypothesis DMS produced by phytoplankton in the ocean was considered as the precursor for CCN in the MBL. The CCN produced were investigated for their cloud producing properties and the subsequent change in planetary albedo. The feedback loop, as seen in figure 3.3, was closed by linking the DMS precursor dimethylsulphoniopropionate (DMSP) to a survival trait of the phytoplankton.

Anthropogenic sources were ignored as the regions the hypothesis focussed on were remote, while other natural gaseous sulphur producers were considered insignificant. The purpose for phytoplankton's production of DMS was suggested to be from DMSP, used in osmo-regulation and the cycle for methionine (Vairavamurthy et al., 1985). The highest flux of DMS from the ocean to the atmosphere was concluded to occur in the most saline, hottest and sunlit areas. The formation of sub-micrometer NSS sulphate particles was attributed to the oxidation of DMS by hydroxide. Other reactions removing DMS to non CCN forms were considered too low to have a significant effect. From here it was concluded that increases in DMS flux from the ocean directly increased the number of CCN present in the form of NSS sulphate aerosols (Charlson et al., 1987).

3.2. DIMETHYL SULPHIDE, AEROSOLS AND THE ENVIRONMENT

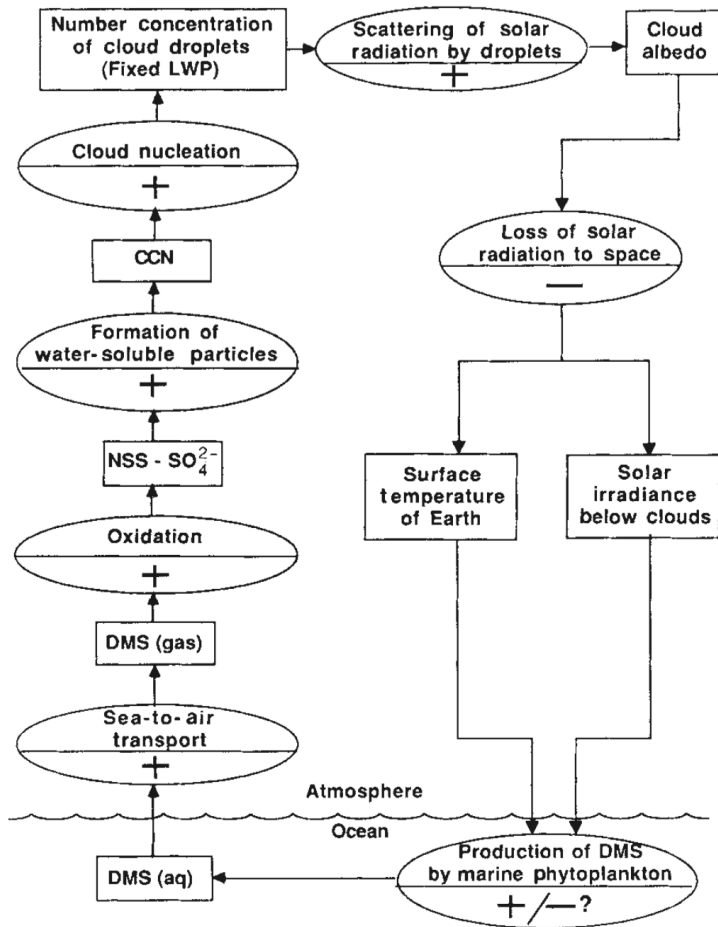


Figure 3.3: The original feedback loop diagram describing the CLAW hypothesis postulated in the paper by Charlson et al. (1987). Rectangles are measurable quantities, ovals are processes. The sign indicates the effect a positive change in the previous rectangle has on the next rectangle. The appearance of both signs in the production of DMS oval reflects the author's uncertainty of this particular effect. If it is positive, then the diagram describes a negative feedback loop, stabilising the climate.

Charlson et al. (1987) attempted to establish NSS sulphate as the prominent CCN in the remote marine atmosphere and that higher concentrations increased or altered the reflective properties of cloud cover and thus albedo. NSS sulphate particles derived from DMS were considered to be in the right size range and have the correct properties for acting as CCN. They used a model developed by Twomey (1977) to predict the change in albedo from the change in the number of CCN. By keeping the water content constant and increasing the number of CCN, the mean radius of the droplets formed decreased. However the overall surface area of the droplets increased, thereby increasing cloud albedo. The model was used along with top of cloud satellite data to predict a change of 0.016 to planetary albedo from a 30 %

increase in CCN.

The final part of the loop involved the DMSP production mechanism and an attempt to link phytoplankton species that emit large amounts of DMSP with increased survival. A number of possible explanations were put forward, such as increased ocean salinity during ice ages, as DMSP protects against dessication. The resulting accidental formation of CCN may have acted as a further survival mechanism. This completes the hypothesis that a negative feedback mechanism exists where increases in the Earth's temperature increases planetary albedo which then decreases the Earth's temperature (Charlson et al., 1987).

An analysis of aerosol data collected at Cape Grim in Tasmania was one of the first attempts to experimentally validate the CLAW hypothesis (Ayers et al., 1991). Ayers et al. (1991) compared concentrations of methane sulphonic acid (MSA) and concentrations of CCN. MSA was considered a relevant surrogate for DMS in the absence of long term DMS data. The results showed a correlation between MSA and CCN concentrations along with seasonal dependence. Interestingly, there was a period during winter where MSA dropped close to zero while CCN did not, indicating the presence of an unknown CCN source. The relationship between MSA and CCN was found to be non-linear. This experiment showed that the production of CCN from phytoplankton aspect of the CLAW hypothesis was at least plausible.

3.2.2 Post-CLAW Research

The CLAW hypothesis has prompted a large amount of research and experimentation. Quinn et al. (2011) explored this research and formed the view that the hypothesis has been invalidated. The three core elements of the CLAW hypothesis were identified as follows: a significant proportion of CCN in the MBL must be DMS derived, changes in DMS derived CCN cause changes to cloud albedo, and DMS production is affected by ocean surface temperatures and solar radiation changes due to cloud albedo (Quinn et al., 2011). The final cycle proposed by Quinn et al. (2011) can be seen in figure 3.4.

Quinn et al. (2011) identified two primary CCN competitors, sea salt particles and primary organic particles. A significant amount of MBL CCN were found to have a sea salt nucleus. Experiments where particles were heated past 600 °C reported 20 % refractory particles sourced at 400 m across the Atlantic, and 40 % aboard a research ship in the north-east Atlantic. Sea salt particles are likely to be the only refractory particles present (O'Dowd et al., 1993). Sea salt particles were also found to make up 60 % of evaporated cloud droplets. The difference in these percentages is because

3.2. DIMETHYL SULPHIDE, AEROSOLS AND THE ENVIRONMENT

sea salt particles act as CCN at lower supersaturations (Tang et al., 1997).

Primary organic particles are aerosolised through the same mechanism as sea salt, but the constituents come from the detritus of organisms which collects on the ocean surface. The larger organic particles may break up in the atmosphere due to UV exposure or acidification. According to measurements recorded in the North Atlantic ocean, mass concentration of these particles increased during bloom periods (O'Dowd et al., 2004). Organic particles (and sea salt) may also scavenge DMS products, which removes their effect on CCN concentrations, if the scavenging particle was already acting as a CCN. Due to the seasonal nature of primary organic particles, they may account for some of the seasonal relationship originally found by Ayers et al. (1991), between DMS and CCN concentrations.

For the remaining DMS derived particles, direct nucleation of DMS products likely occurs at the top of clouds, in the FT. Clouds remove existing particles in this region, which decreases the available surface area, and promotes homogeneous nucleation (Perry et al., 1994). Deep convective clouds also move DMS up into the FT (A. Clarke et al., 1998). The faster winds present in the FT would move the particles away from the DMS's origin, breaking the localisation required for the feedback loop. Quinn et al. (2011) argues that the majority of DMS derived particles present in the MBL are from this process.

Cainey et al. (2007) similarly identified three main ideas through which the feedback mechanisms of the CLAW hypothesis have been diminished. These are: the effectiveness of DMS to become CCN, the prevalence of sea salt particles in the CCN size range, and the direct aerosolisation of organic particles from the ocean surface through bubble bursting.

The effect that aerosols have on cloud albedo is more complicated than the direct relationship proposed in the original CLAW hypothesis (Quinn et al., 2011; Cainey et al., 2007). An increase in cloud albedo can be countered by a decrease in cloud fraction through improved entrainment of sub-saturated air around the cloud (Zuidema et al., 2008). Charlson et al. (1987) predicted a 1.3 °C decrease in surface temperature for a 30 % increase in CCN. As the extra CCN are unlikely to be entirely DMS derived, the required increase in DMS flux would need to be very high, around 300 % according to values modelled by Woodhouse et al. (2010).

An alternative action through which DMS derived sulphur compounds are removed, and thus prevented from becoming CCN directly, is through heterogeneous nucleation onto existing particles (Cainey et al., 2007). Such an action may work to alter the chemistry of the particle and thus the albedo of the clouds formed from them. This

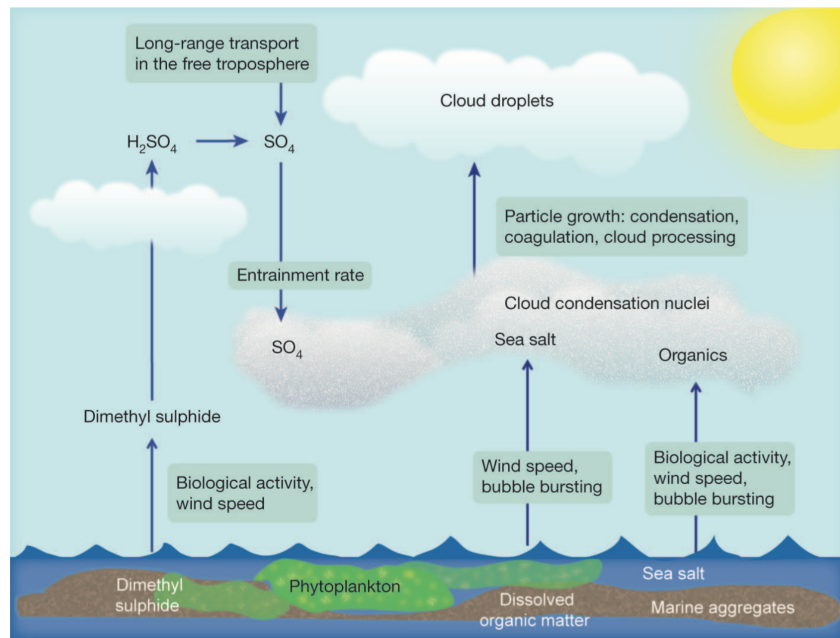


Figure 3.4: An updated cycle for CCN production in the MBL. Major changes to the cycle in figure 3.3 are nucleation in the FT driven by clouds, and the presence of sea salt and primary organic aerosols (Quinn et al., 2011).

may provide an alternate way for DMS to affect climate.

Quinn et al. (2011) advise that the CLAW hypothesis should be retired, but acknowledge its impact in developing this area of science. Other mechanisms of climate regulation may still be present, such as sea salt particle concentration increases with wind speed, and primary organic particles with biological production. Cainey et al. (2007) take a more compromising stance, advising that research into the CLAW hypothesis is still on-going and current results need to be fully implemented in modelling.

3.2. DIMETHYL SULPHIDE, AEROSOLS AND THE ENVIRONMENT

4. The Great Barrier Reef

The Great Barrier Reef (GBR) is the world's largest organic structure. The marine park encompassing it is 344 400 km² (see figure 4.1), of which around 6 % is comprised of 2900 separate coral reefs (Borthwick et al., 2006).

Climate change is causing an increase in sea surface temperature (SST), which effects coral survival in the GBR (Hoegh-Guldberg, 1999). Most corals rely on a symbiotic relationship with algae for energy, but when sufficiently stressed, the algae is ejected, this is coral bleaching (Hoegh-Guldberg, 1999). Stresses associated with changing conditions, and bleaching events, may also impact coral's production of DMS (Raina et al., 2013).

Satellite imagery has been used to try and establish a link between SST and cloud coverage in the GBR. Leahy et al. (2013) found relationships where changes in SST was responsible for changes in cloud cover, but also that cloud cover was responsible for changes in SST. Both were found to have a three day delay. The SST to cloud cover correlation implies a negative feedback mechanism for cloud formation, with DMS produced by stressed coral mentioned as a possible source (Leahy et al., 2013).

4.1 Coral DMS Production

While the CLAW hypothesis was based only on phytoplankton as a producer of DMS, phytoplankton are not the only organisms responsible for its production. DMSP production by coral is another source. Research has been performed on the effects of ocean temperature changes (G. Jones et al., 2007), and the role of Symbiodinium (the algae that lives inside coral in a symbiotic relationship) in DMSP production (Raina et al., 2013). DMSP is converted to DMS by bacteria in the ocean (Todd et al., 2007).

Separate research on DMSP production by Symbiodinium, and adult coral, had

4.1. CORAL DMS PRODUCTION

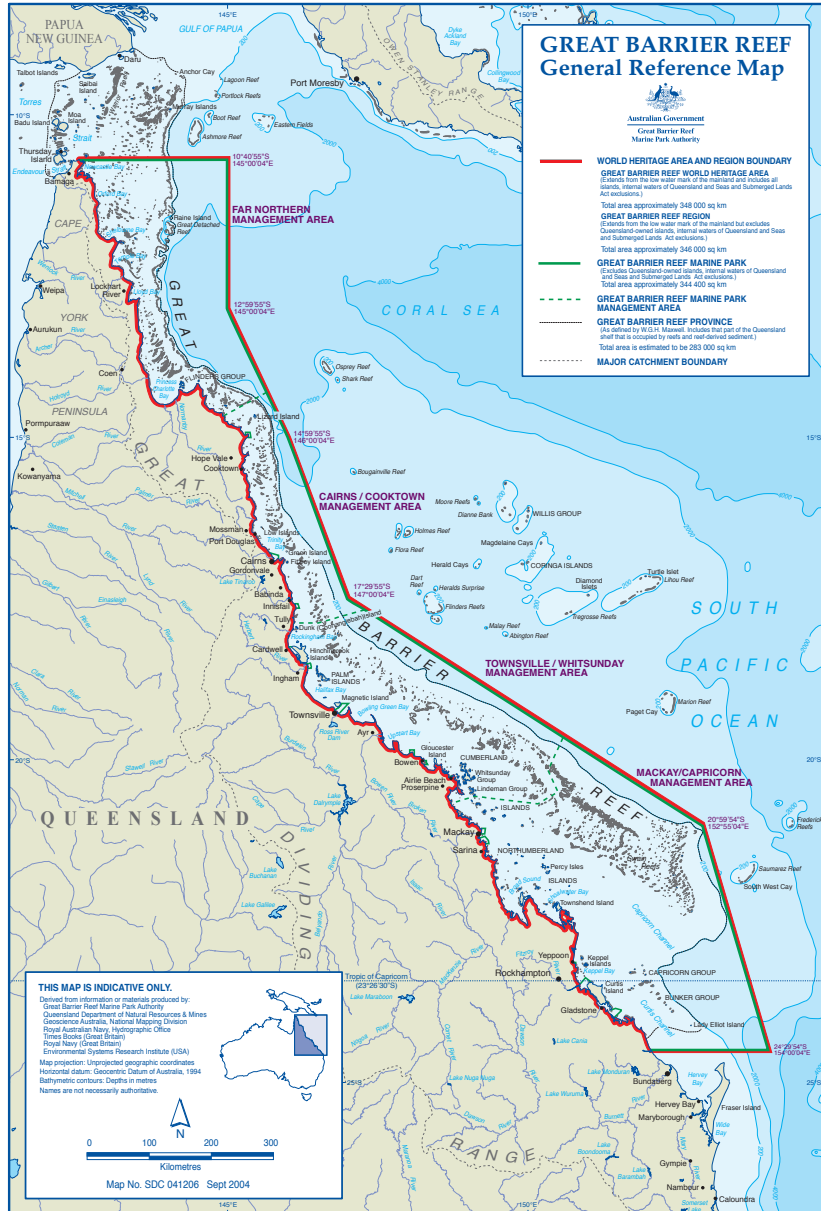


Figure 4.1: The boundary of the Great Barrier Reef Marine Park illustrating the extent of its coverage along the Queensland coast (Borthwick et al., 2006).

previously shown a discrepancy in total DMSP production. Experimentation on the larval phase of coral yet to be inhabited by Symbiodinium has shown that coral larvae produce DMSP independently (Raina et al., 2013). DMSP concentration from coral was also found to be two times higher than that produced by benthic algae common to the GBR (Raina et al., 2013).

An increase in temperature has been found to result in an increase in coral DMSP production (see figure 4.2). DMS is known to have antioxidative effects, implying that increased DMSP production is a defence against damage caused by heat stress. Adult colonies whose Symbiodinium was destroyed by heat stress also produced increasing levels of DMSP with increasing temperatures. Prior to Raina et al. (2013), it was assumed that increasing temperatures killing off the Symbiodinium would quickly decrease DMSP production. This no longer appears to be the case.

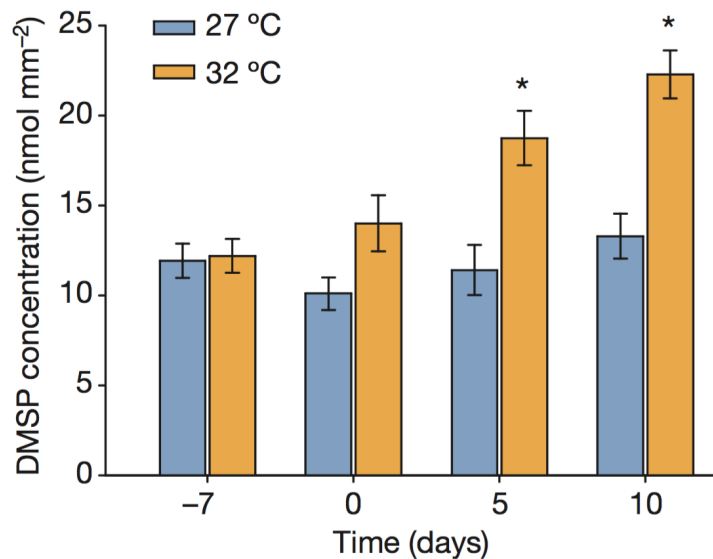


Figure 4.2: Adult coral DMSP production increases when stressed by a higher temperature over an extended time period (Raina et al., 2013).

If DMSP concentration has a resulting effect on cloud formation through CCN, changing coral cover due to changing climate may impact local climate regulation.

4.2 GBR DMS Production

Coral's eventual production of DMS in the GBR region has been explored experimentally. Results from the GBR indicate that corals can produce very high concentrations of DMS and DMSP (Broadbent et al., 2004). These concentrations also appear to depend on SSTs, and on tidal levels (G. Jones et al., 2007). The extent of the GBR presents a large source of sulphur that enters the atmosphere (G. B. Jones et al., 2005).

The GBR region is exposed regularly to south-easterly and southerly trade winds, providing the wind shear required to transfer DMS from the ocean to the atmosphere

4.2. GBR DMS PRODUCTION

(Liss, 1983). During a voyage in 1997, G. B. Jones et al. (2005) measured the highest levels of atmospheric DMS when these trade winds passed over large areas of the reef experiencing low tides (see figure 4.3).

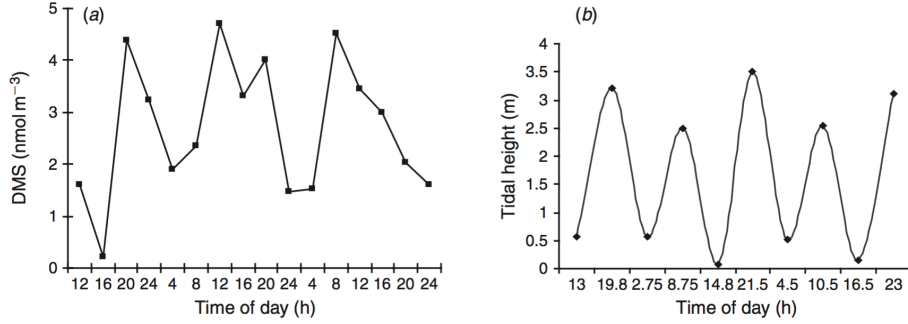


Figure 4.3: Data indicating the presence of a delayed link between atmospheric DMS concentrations and low tide events in the northern GBR and NW Coral Sea (G. B. Jones et al., 2005).

From here the production of CCN from GBR sourced DMS is not as well established. Much depends on the meteorology of the region and the relative concentrations of competing CCN and DMS sinks. Localised modelling is needed to provide predictions in this area of research (Cainey et al., 2007).

5. Modelling

The complexity of the atmosphere and the processes within it, detailed in chapter 2, require modelling to produce theoretical descriptions of the systems. Generally, a number of models are chained together to simulate different parts of the climate system. Each of these models is built upon a number of theories that are used depending on the state of the system at the time (Jacobson, 2005, Chapter 21). This complexity makes atmospheric modelling difficult and broad. Fortunately many models have been developed around the world to fill niches such as HYSPLIT for trajectory modelling, the Unified Model for climate and weather modelling and CCAM for atmospheric modelling (Draxler et al., 1997; Mann et al., 2010; Cope et al., 2009; McGregor et al., 2008).

The first choice to make when deciding which model to use is between a Global Climate Model (GCM) and a Regional Climate Model (RCM). The difference is in the granularity achieved in the discretisation used to solve the governing equations, and the requirements of boundary conditions (Thatcher et al., 2015). A RCM is run on a smaller scale for a specific region with a high density of grid points. As only a small portion of the Earth's surface is simulated, the values of parameters at the boundary of that region must be known in advance (Hurley, 2002). Usually these boundary conditions are obtained from a previous run of a GCM. Although a GCM is less restrictive than a RCM, its lack of high resolution may miss small but critical details. Conversely, the regional restriction of a RCM can miss distant events that may influence the climate in the simulated region (Seinfeld et al., 2012, Chapter 25).

5.1 Back Trajectory Modelling

When working in atmospheric science, it is often necessary to model the trajectories that parcels of air travel. With the advent of large scale meteorological measurements, the data required to model this process is now being produced. Trajectory modelling

5.2. CCAM, CTM, GLOMAP

is able to take a particular location and predict, forward or backward in time, the path a parcel of air travels to or from that location. It can be used to predict whether air at a particular location has passed over a region or event of interest or, for example, whether there has been contamination from anthropogenic sources (Draxler et al., 1998). HYSPLIT is one such trajectory model. HYSPLIT's efficacy in performing back trajectory modelling is well established (Draxler et al., 1998). It has been used to model many different scenarios from forecasting fire smoke movement (Glenn D Rolph et al., 2010) to nuclear cloud dispersion (G D Rolph et al., 2014).

5.2 CCAM, CTM, GLOMAP

For modelling the full aerosol pathway, from atmospheric, to chemical transport, to aerosol microphysics CSIRO uses a trio of models: CCAM, CTM and GLOMAP-mode. This combination of models has been used previously in the Sydney Particle Study (Cope et al., 2014). The Sydney Particle Study was a large scale study performed by seven different organisations and lead by CSIRO. It encompassed both measurement and modelling of fine particles in the Sydney area, with a view to understand their exposure to Sydney's population. Both CCAM and TAPM (an alternative meteorological model produced by CSIRO) were used as the RCMs for the study. Their outputs were compared with each other, and with the collected data. CTM, and consequently GLOMAP-mode, were used for the particle dynamics and chemical transport modelling within the two RCMs. Both RCMs performed well, with predictions of sea salt, organic matter and secondary inorganic aerosols within 15 % of observations (see figure 5.1) (Cope et al., 2014).

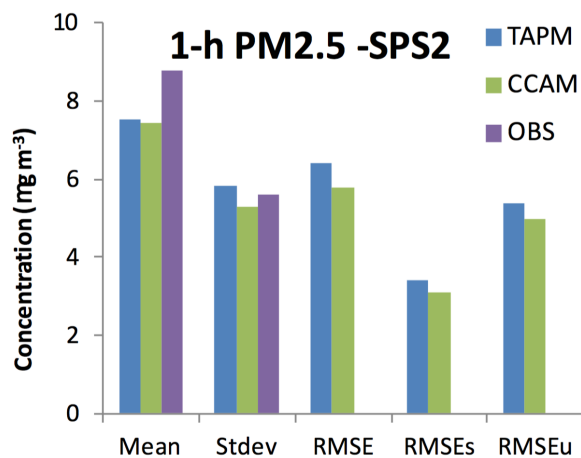


Figure 5.1: The hourly averaged concentrations of PM_{2.5} particles for the second Sydney Particle Study. Both CCAM and TAPM used as the base meteorological model produce similar average concentrations, close to observation (Cope et al., 2014).

5.2. CCAM, CTM, GLOMAP

6. DMS Climatology Modelling

The way in which DMS is created and enters the atmosphere needs to be considered when attempting to model its effects on climate. There are a number of ways in which this can be treated: using large data maps, modelling the ocean, and/or applying different methods for ocean surface-to-atmosphere exchange (surface flux) (Woodhouse et al., 2010). These climatological models of DMS are needed to produce the chemical concentration maps used as input for any chemical transport model (see section 7.1.3).

6.1 Modelling DMS production

A number of studies exist for modelling DMS. Their methods provide guidance for which modelling systems are successful, and which DMS climatological models are necessary to produce realistic results.

The Pacific Atmospheric Sulfur Experiment (PASE) measured DMS and SO₂ levels via flights made at 40 m above sea level in the remote Pacific Ocean, near Christmas Island (Bandy et al., 2011). Other chemicals were also measured, including H₂SO₄. Using this data Simpson et al. (2014) devised budgets for DMS, SO₂ and NSS sulphate particles. The DMS budget consisted of surface flux, entrainment, oxidation and divergence. Using the budgets it was calculated that approximately 20 % of DMS became NSS sulphate particles.

In the region measurements were taken from, an easterly jet stream from South America introduced NSS sulphate particles, originating from the land, into the MBL. This was exacerbated by a localised subsidence. Modelling showed that the particles introduced via FT entrainment dominated those produced from DMS for the region (Simpson et al., 2014). The study revealed that their results were influenced by regionally specific inputs that may not be present in the GBR, and highlights the importance of localised modelling and the potential influence of particles from the FT (Simpson et al., 2014).

6.2. DMS SURFACE FLUX

Woodhouse et al. (2010) produced a global model of DMS and its effects on CCN concentration. Aerosol processes were modelled using GLOMAP-mode inside of a chemical transport model called TOMCAT. A number of DMS climatologies were tested, with the climatology developed by A. J. Kettle et al. (2000) as a reference point (see section 6.2). The model showed that DMS's highest impact on CCN was in the southern hemisphere (see figure 6.1). Also, any region with large anthropogenic CCN sources sees little impact from DMS (Woodhouse et al., 2010). Overall, the global impact of DMS on CCN in the model was low. It was also found that changes to CCN production from different climate change scenarios could not be distinguished from variances arising from using different climatology models.

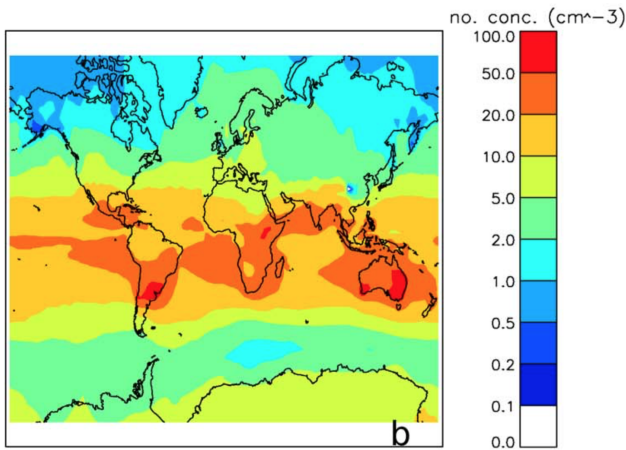


Figure 6.1: A global map of the difference between CCN concentrations produced by model runs with and without DMS (Woodhouse et al., 2010).

6.2 DMS Surface Flux

As mentioned in section 7.1.3, maps of the chemicals being analysed are required to feed into any chemical transport model used. For DMS, this is often given as a surface flux map for the region of interest. There are many meteorological and biological variables influencing DMS surface flux. The major meteorological variable is wind speed at the surface of the ocean (A. J. Kettle et al., 2000). Surface concentrations of DMS are generally taken from experimental data with a flux model producing atmospheric concentrations (Woodhouse et al., 2010).

A. J. Kettle et al. (2000) describes a methodology for approximating a global DMS surface flux map. Data was collected from a large number of publications, study databases and direct correspondence with researchers (see figure 6.2). The data

was then interpolated to provide monthly global 1° resolution sea surface DMS maps. Maps for sea surface salinity, temperature and chlorophyll concentration were also created (A. J. Kettle et al., 1999). In A. J. Kettle et al. (2000) the surface concentration maps from A. J. Kettle et al. (1999) were converted to surface flux maps using a technique from Liss (1983). The transfer rate was assumed to be a function of the concentration difference between the ocean and air, and the piston velocity, which depends on wind speed. Other surface flux methods were also examined and the differences between them produced an error in DMS results greater than 50 %. Overall, the method showed little dependence on meteorological changes to DMS flux, around 10 % for future predicted changes.

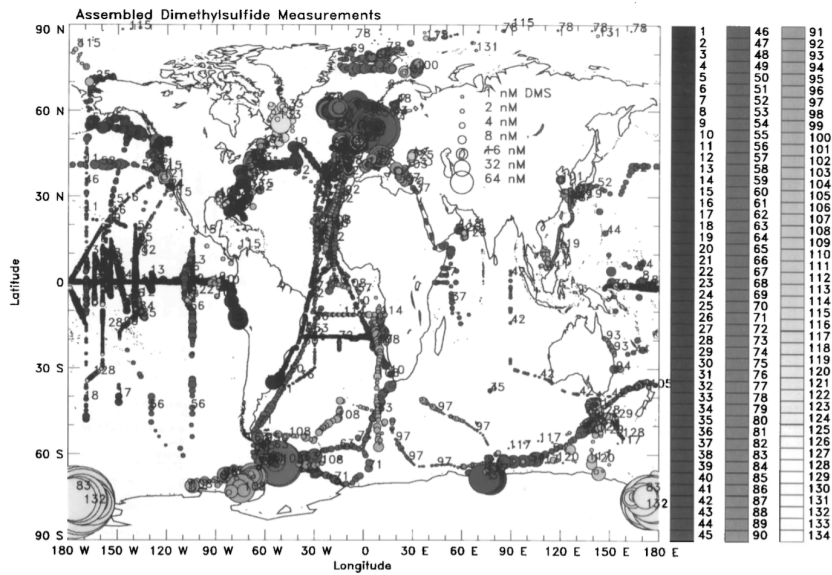


Figure 6.2: The global measurement data used for producing interpolated maps of DMS sea surface concentrations (A. J. Kettle et al., 1999). Larger circles indicate higher concentrations while shading defines the contributor.

Lana et al. (2011) expanded on this work producing a more complete and accurate climatological model of DMS surface flux. Their model indicates a summer increase in surface flux (see figure 6.3) and also a vertical dependence on atmospheric DMS concentration. The database of measurements used was also three times larger than that of A. J. Kettle et al. (1999), resulting from continued efforts into the SOLAS project (Surface Ocean Lower Atmosphere Study) (Lana et al., 2011).

The observational data for the GBR was largely sourced from G. B. Jones et al. (2005). Interestingly, both ocean surface and atmospheric DMS concentrations were measured in this study. The significance of a regional and diurnal dependence on DMS concentrations indicates that the global results obtained in Lana et al. (2011) should not be assumed for regionally specific models.

6.2. DMS SURFACE FLUX

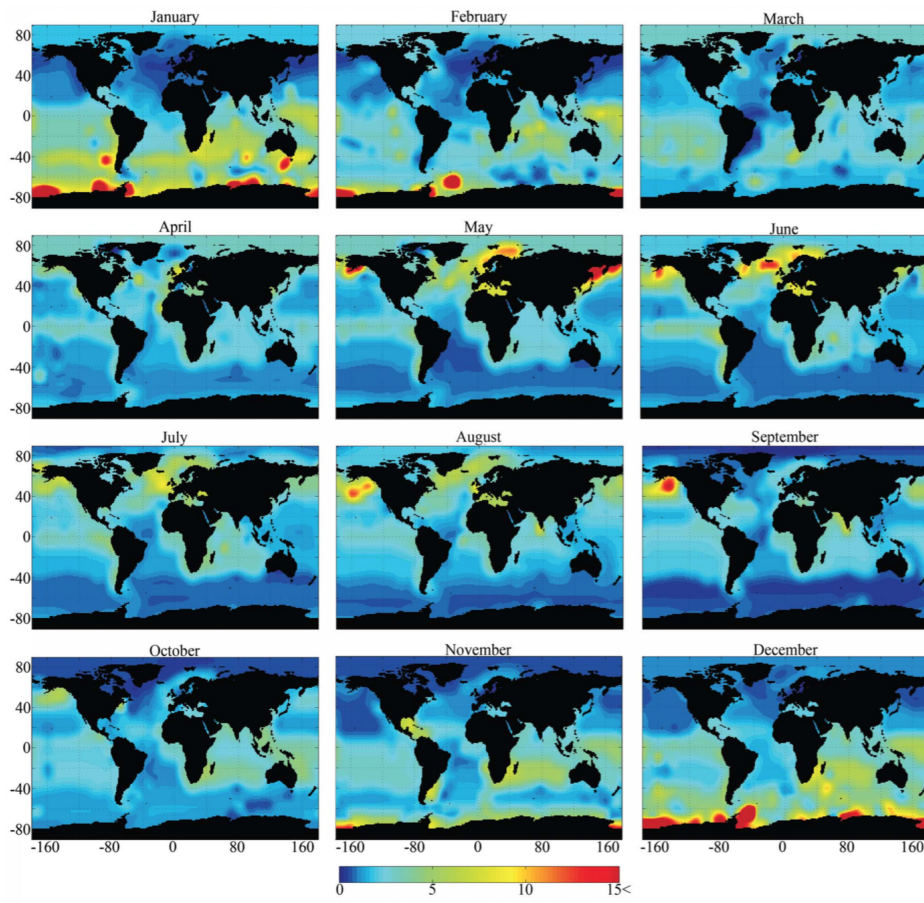


Figure 6.3: Monthly global maps of DMS concentrations produced using surface concentrations and an updated surface flux parameterisation (Lana et al., 2011). Increases in DMS concentrations during summer periods can be seen.

Part II

Research

7. Methodology

7.1 Models

The first part of this project involves modelling the source of air at particular locations. For this HYSPLIT was used as it is an established back trajectory model (see section 5.1). The three models used in the second part of this project were CCAM, CTM and GLOMAP-mode (see section 7.1). CCAM provides the meteorological data needed for CTM and CTM provides the chemical concentration data required for GLOMAP-mode. However, currently the system is limited to running CCAM offline from the other models (see figure 7.1) (McGregor et al., 2008). Thus there is no feedback into the meteorology from changes in chemical or aerosol levels, such as cloud production caused by changes in CCN concentrations.

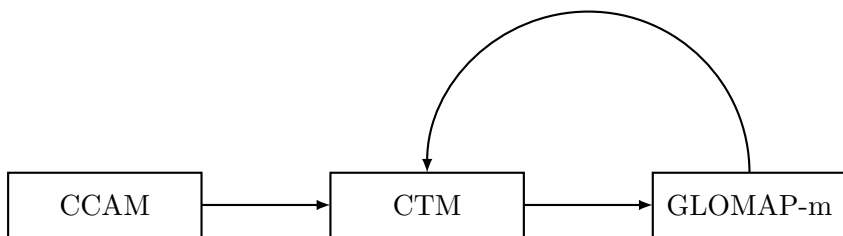


Figure 7.1: The group of models prepared by CSIRO for modelling from meteorology to aerosols. Arrows indicate the direction data passes.

7.1.1 HYSPLIT

HYSPLIT is the Hybrid Single Particle Lagrangian Integrated Trajectory model developed by the National Oceanic and Atmospheric Administration and Australia's Bureau of Meteorology. It takes as input a variety of different meteorological data sources to produce the field the parcel of air being tracked travels through.

7.1. MODELS

A Lagrangian model may be implemented in two different ways. A puff model regularly releases and follows a parcel of air containing the required fraction of trace components. The puff moves and expands depending on advection and diffusion respectively. A particle model releases many single particles which are moved through advection, but which are also randomly moved based on the diffusion present (Draxler et al., 1997). HYSPLIT implements a hybridisation of these models by using the particle style for vertical motion, and the puff style for horizontal motion (Hurley, 1994).

The user provides a location and time for the start of the trajectory, and the amount of time backwards or forwards for it to run. HYSPLIT produces a line of latitude and longitude points where each point is an amount of time away from the starting time. Thus the line through the points indicates the trajectory, backwards or forwards through time of the air at the starting location.

HYSPLIT, like all atmospheric models, is sensitive to initial conditions (Challa et al., 2008) and its accuracy is dependent on the error margins of the meteorological data it makes use of (Draxler et al., 1998). The results of any trajectory run are therefore less accurate the further away from the initial conditions the trajectory gets. There is also a dependence on the spatial and temporal granularity of the meteorological data. As such, HYSPLIT offers the ability to slightly permute the initial conditions of the model to produce a multitude of possible trajectories for a single location and time (Draxler et al., 1997). It is also possible to produce multiple trajectories over time or over space and a robust scripting platform exists to allow this (Draxler et al., 1997).

HYSPLIT Visualisations

A technique for producing meaningful visualisations of this modelling system, given it's shortcomings, is to produce a normalised histogram of multiple trajectories. The GUI side of HYSPLIT offers a method for doing this using the bulk production of trajectories from permuted initial conditions (Draxler et al., 1997). A spatial domain is subdivided into boxes, then whatever points of the various trajectories that lie in that box are counted. Each box is then normalised by the total number of trajectory points in the domain. It is then possible to plot these boxes onto a map of the region, colouring them based on their values. This technique provides a visual idea of whether a given parcel of air will have passed over that box. Similarly, by producing multiple trajectories over time, it is possible to create a visualisation of the likelihood that a parcel of air has passed through a box within a time period.

If the number of points in box i is N_i then the fraction of the total points being in that box f_i is given by,

$$f_i = \frac{N_i}{\sum_{i=1}^m N_i}, \quad (7.1)$$

where m is the total number of boxes (Lefebvre, 2006, Chapter 3).

Another visualisation tool is to create a time series of the trajectories, overlaid on a map, in a movie. This shows how the trajectory evolves with the changing meteorological conditions. This could be coupled with the interpolated histograms computed using small variations of the initial conditions to produce a better idea of probable trajectories' evolution through time.

7.1.2 CCAM

CCAM is CSIRO's Conformal-Cubic Atmospheric Model. Most RCMs are performed on a grid that simulates only the area of interest, requiring spatial boundary conditions to be fed into the model at each time step (Hurley, 2002). Because of CCAM's approach of conformal cubic mapping, the majority of grid points can be focussed onto the region of interest while still simulating the rest of the globe with a gradient of accuracy (see figure 7.2). This removes the necessity for boundary conditions as the full globe is being simulated, which allows distant events to influence the region of interest. However, there are fewer grid points in distant regions, sacrificing accuracy for computation time (McGregor, 2005).

As inputs CCAM can accept data sets from a GCM and nudge the model towards these values (McGregor, 2005). Although work is being done to incorporate a coupled ocean model with matching grid structures, without this the oceanic parameters, such as sea surface temperature, must be input as both spatially and temporally varying maps (McGregor et al., 2008). Despite the non-uniformity of the cubic grid structure, CCAM produces latitude and longitude based output through interpolation of the cubic grid data (Thatcher et al., 2015).

The current implementation of CCAM uses a semi-Lagrangian solver that is semi-implicit and non-hydrostatic, programmed in FORTAN. The solver is designed for expansion to a large number of cores, while dealing with the singularity-like points caused by the cubic mapping (Thatcher et al., 2015). It is also possible to run the model multiple times, focussing the grid in at each step while nudging is performed using the previous runs' data (McGregor et al., 2008).

Due to the nature of the grid structure CCAM uses, any domain must be transformed

7.1. MODELS

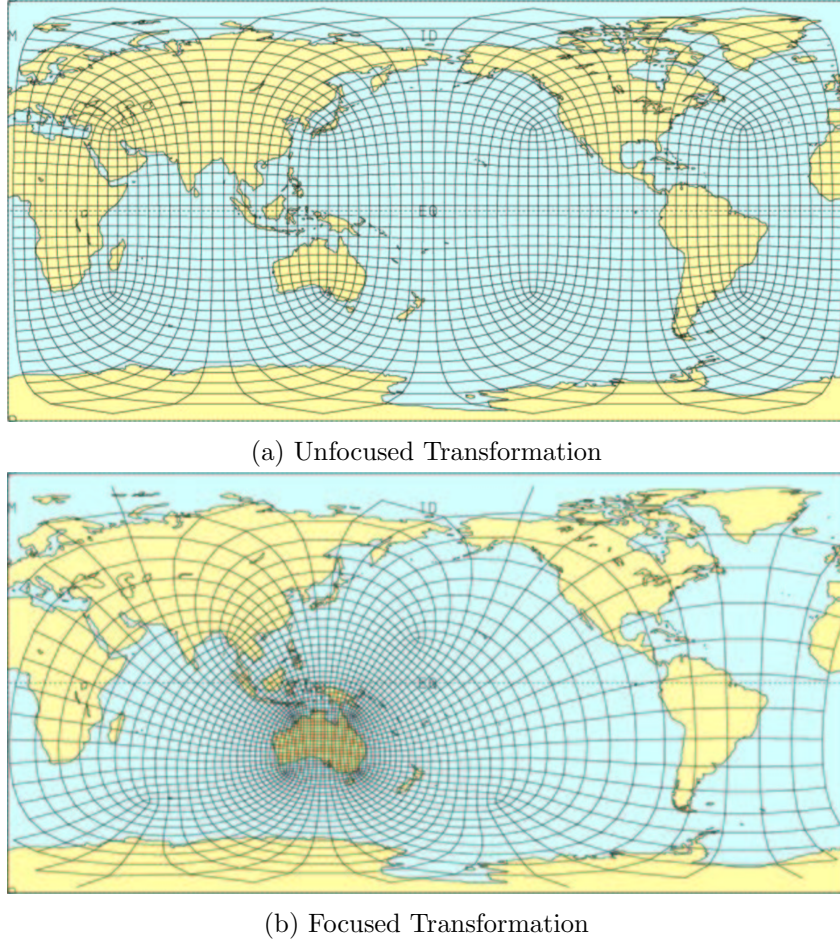


Figure 7.2: Two examples of the conformal cubic mapping, used by CCAM, showing both a focussed and unfocussed transformation of the grid (McGregor, 2005). The focused transformation has a lower Schmidt number than the unfocussed transformation.

to match the inputs CCAM uses. These inputs are the latitude and longitude of the domain's centre, the grid size, and the Schmidt number. The grid size is the number of grid squares horizontally or vertically, as the domain must be square. The Schmidt number scales the front panel of the cube that approximates the globe. So the centre point positions the front face of the cube, the Schmidt number scales the face, and the grid size defines the resolution.

The Schmidt number S is calculated from the length of the domain in degrees L_d ,

$$S = \frac{L_d}{90}. \quad (7.2)$$

The grid size g is calculated through the length of the domain in kilometres L_k and

the resolution, or length of an individual grid square in kilometres R_k ,

$$g = \frac{L_k}{R_k}. \quad (7.3)$$

The grid size chosen greatly effects the parallelisation of the model and thus the runtime (Thatcher et al., 2015). It is best to try and find the closest acceptable grid size, and then modify the Schmidt number to maintain the desired resolution, without changing the size of the domain too much.

7.1.3 CTM

CTM is the Chemical Transport Model produced at CSIRO. It deals with various transport processes relating to chemicals found in the atmosphere, as well as deposition onto particles, changes in chemical structure, and emission sources (Cope et al., 2009). It uses a regular grid structure which requires boundary conditions (see figure 7.3) that are usually taken from a GCM (Cope et al., 2014). The transport of each chemical species is modelled using an advection diffusion equation around the chemical's concentration, with source terms relating to different chemical processes. Each of these are themselves modelled and solved before being fed back into the advection diffusion solver (Cope et al., 2009).

CTM is written in FORTRAN, but allows for chemical reactions to be entered as regular form chemical equations (Cope et al., 2009). It requires a meteorological map as input, along with initial and boundary conditions for each chemical being tracked. Maps for the introduction of chemicals from the surface to the atmosphere are also required, such as when DMS is produced by the GBR. CTM outputs atmospheric maps of chemical concentrations.

CTM defines the domain through the latitude and longitude of the bottom left grid point (BL_{Lat}, BL_{Lon}), the number of horizontal and vertical grid points (n_x, n_y), and the horizontal and vertical distance between grid points (d_x, d_y). Taking a square domain defined via its centre point (C_{Lat}, C_{Lon}), its width and resolution in degrees L_d, R_d , then,

$$d_x = d_y = R_d. \quad (7.4)$$

So,

$$n_x = n_y = \frac{L_d}{d_x}. \quad (7.5)$$

7.1. MODELS

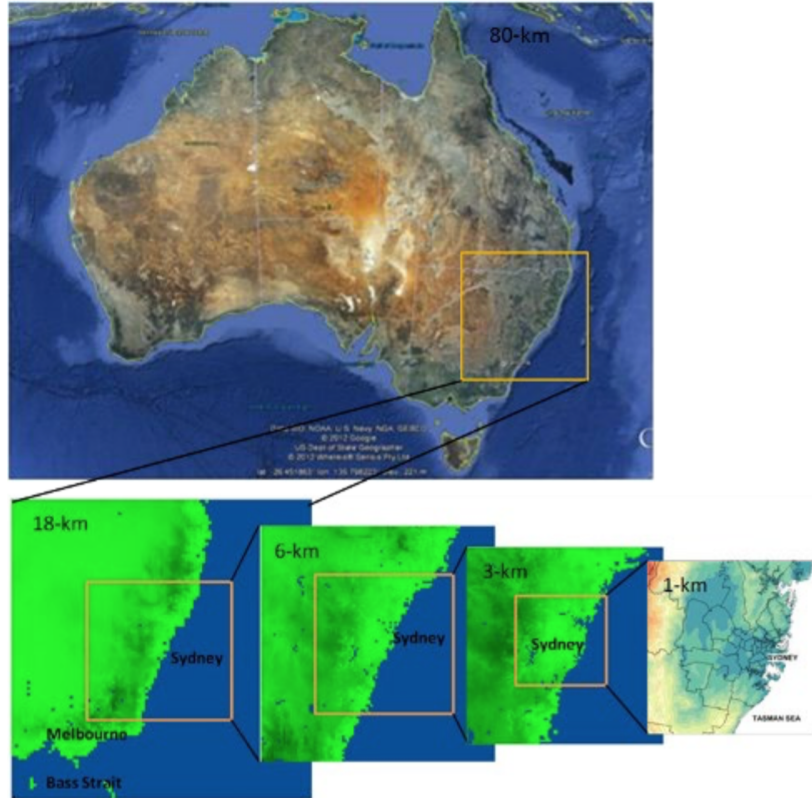


Figure 7.3: A series of the zooming CTM grids used in the Sydney Particle Study. An example of a CTM produced chemical concentration map can be seen at the bottom right (Cope et al., 2014).

Thus,

$$(BL_{Lat}, BL_{Lon}) = (C_{Lat}, C_{Lon}) - \frac{n_x d_x}{2}. \quad (7.6)$$

7.1.4 GLOMAP and GLOMAP-mode

GLOMAP is the aerosol micro-physics component of the UKCA model developed at Leeds university. It uses atmospheric information and chemical concentrations to simulate the large amount of interactions aerosols undergo. It models new particle formation, condensation, cloud processing, hygroscopic growth and many other aerosol processes (Mann et al., 2010).

GLOMAP-mode is an alternate version of GLOMAP which segregates aerosols via modes (see section 2.4) rather than the GLOMAP's direct bin approach. GLOMAP-mode also uses the equilibrium Henry's law style aqueous phase reactions recommended by Barnes et al. (2006), while GLOMAP uses a more computationally

expensive diffusion limited method (Mann et al., 2010). Both differences make GLOMAP-mode less accurate, but also less computationally expensive. Some treatments of particles are also adjusted to better make use of the modal structure. An example is that GLOMAP applies rain-out to any particles over 103 nm, while GLOMAP-mode applies rain-out to soluble particles in the accumulation and coarse modes (Mann et al., 2010). For modelling DMS and its aerosol products, GLOMAP uses the sulphur oxidation steps outlined in Seinfeld et al. (2012) and precomputed Henry’s law coefficients (Mann et al., 2010).

The chemical concentration maps needed to feed into GLOMAP can either be offline, computed beforehand, or online (Mann et al., 2010). Online maps are updated by what is consumed or produced within GLOMAP and then passed to a chemical transport model running above GLOMAP (Spracklen et al., 2003). GLOMAP produces maps of aerosol concentrations, separated into bins or modes depending on the version used.

7.2 Study Design

The modelling work in this project is connected to a number of real world experiments to measure the GBR’s effect on climate. This guided much of the design of the study. A number of land based research centres along the Queensland coast needed to be assessed for viability, to see if the majority of the air they received passed over the GBR. A ship voyage was also planned off the coast of Queensland, providing a second series of locations to assess. Back trajectory modelling would be used to study the source of air at these experimental locations. It is important for the locations chosen to have minimal influence from land based aerosol sources as those sources will dominate DMS derived particles. The final chosen locations of the experimental work, directed by this back trajectory modelling, in turn established the position and size of the domains for the aerosol modelling.

7.2.1 Assessing Locations

The visualisation technique proposed in section 7.1.1 was developed to examine the source of air at a location. HYSPLIT was used for modelling back trajectories. To produce the mass back trajectories needed for creating the histogram, a script was developed for running HYSPLIT a large number of times. Alongside this, visualisation scripts to produce the normalised histograms were created.

7.2. STUDY DESIGN

A number of locations both on and off the coast of Queensland were selected (see ??). Back trajectories were modelled at 4 hourly intervals with each trajectory spanning back 120 hours. Year long runs were performed first to gauge the best months. Four years were modelled, from 2011 to 2014. To produce the monthly plots the trajectories from all four years, for each month, were collected and processed to create histograms based on latitude and longitude. The histograms were interpolated and plotted over a map of Queensland.

Table 7.1: *The list of experimental coastal locations along the Queensland coastline that HYSPLIT was run for.*

Name	Latitude	Longitude
Whitsundays	-20.06	148.95
AIMS Cape Ferguson	-19.27	147.06
Orpheus Island	-18.63	146.50
Lucinda Jetty	-18.52	146.39
Cairns	-16.88	145.94
TCU Daintree Forest Observatory	-16.10	145.44
Lizard Island	-14.67	145.45

Table 7.2: *The list of experimental ship locations between the GBR and QLD coastline that HYSPLIT was run for.*

Name	Latitude	Longitude
Mackay	-21.12	149.71
Hamilton	-19.98	149.11
Townsville	-19.24	147.67
Great Palm Isl	-18.62	146.72
Innisfail	-17.53	146.23
Cape Tribulation	-16.09	145.56

7.2.2 CCAM and CTM Domains

As both CTM and CCAM approach defining domains differently, a series of initial domains were chosen. The centre point was selected to be $-19.62, 148.36$, latitude and longitude, using square domains with width 6000, 2000 and 1000 km, with

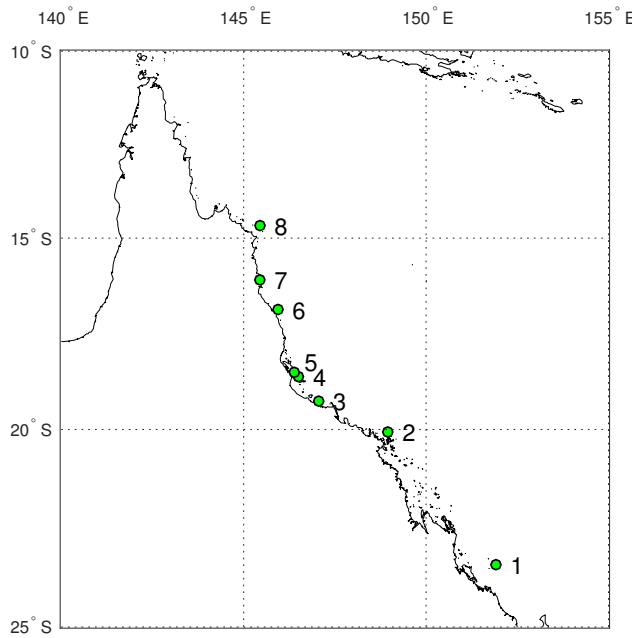


Figure 7.4: The series of coastal locations chosen for modelling back trajectories.

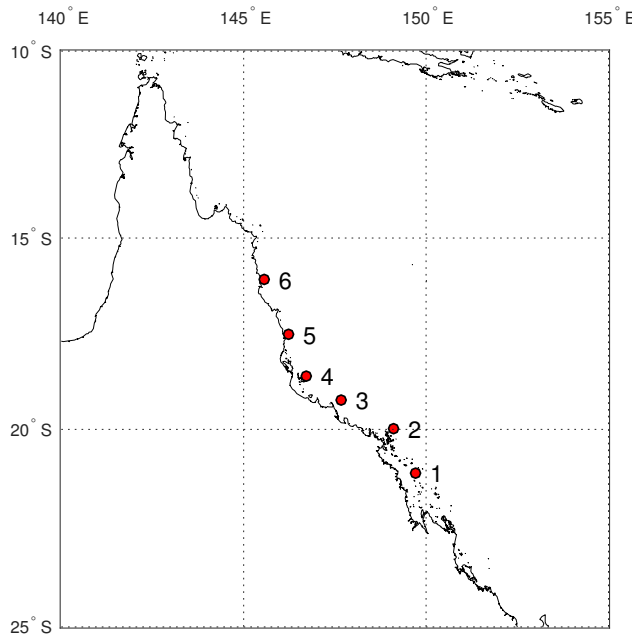


Figure 7.5: The series of ship based locations chosen for modelling back trajectories.

resolutions of 80, 9 and 3 km respectively. The tiered domain structure, with decreasing width but increasing granularity, allows for greater detail at the coastal

7.2. STUDY DESIGN

level. Distant effects, from inland Australia and out to the Pacific Ocean, are still simulated but with lower acuity. This approach attempts to ensure all the important influences are modelled without requiring exorbitant computation times.

Applying the equations in section 7.1.2 and section 7.1.3 produces the domains for each model. The CCAM domain was calculated first, and the CTM domain was calculated from the CCAM domain after shrinking it by 90 %. This was done to avoid the singularities at the corners of the CCAM domain.

Table 7.3: The values defining the domains used in CCAM for modelling the atmosphere over the Great Barrier Reef

Name	Centre Latitude	Centre Longitude	Grid Size	Schmidt Number
GBR 1	-19.62	148.36	72	0.6
GBR 2	-19.62	148.36	288	0.2
GBR 3	-19.62	148.36	384	0.1

Table 7.4: The values defining the domains used in CTM for modelling the chemical transport and aerosol micro-physics over the Great Barrier Reef

Name	Bottom Left Latitude	Bottom Left Longitude	Number of Grid Points	Distance Between Grid Points
GBR 1	-43.385	124.595	50	0.97
GBR 2	-27.62	140.36	81	0.2
GBR 3	-23.6325	144.3475	108	0.075

The first domain, GBR 1, was chosen to capture long range effects within CCAM and CTM. It encompasses the majority of Australia and out into the Pacific Ocean. The back trajectory modelling performed in the GBR influenced the choice of the domains centre, and the size of the final domain. As seen in figure 8.2, the majority of the back trajectories come from the East and South-east. A location along the Queensland coast, with the greatest body of reef towards the East South-east of it, was chosen as the centre point (see figure 7.7). The final domain GBR 3 includes both a portion of the Queensland coast-land, and the majority of the reef to the East South-east.

The CTM domains were shrunk by 10 % of the the CCAM domains, to avoid the

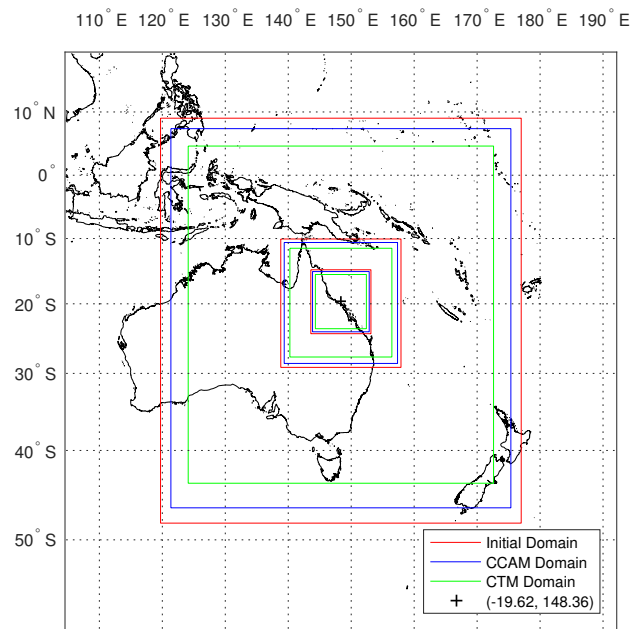


Figure 7.6: A series of three tiered initial domains with their accompanying CCAM and CTM domains.

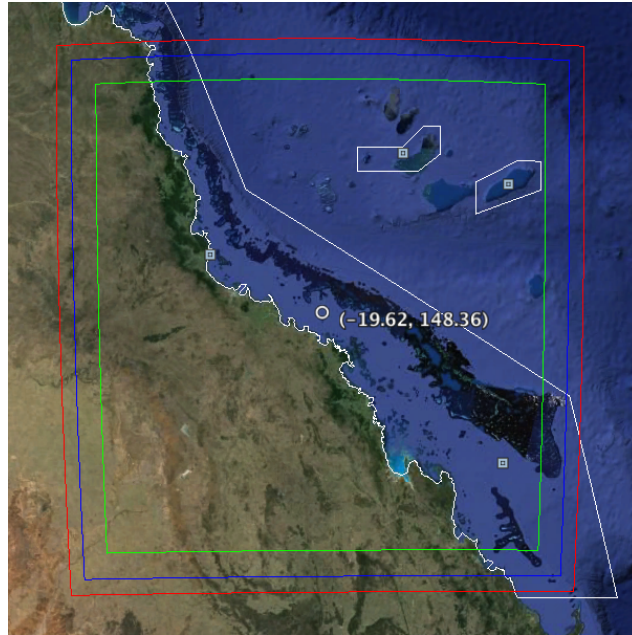


Figure 7.7: The final domain chosen (red) with its calculated CCAM (blue) and CTM (green) domains overlaid onto the globe. The Great Barrier Reef Marine Park is shown in white.

7.2. STUDY DESIGN

singularities at the corners of the CCAM domains. There are other differences on top of this 10 % margin that are a result of the way the domains had to be calculated for CCAM and CTM. The equations illustrated in section 7.1.3 and section 7.1.2 were used for these domain calculations.

7.2.3 Running the Models

The CSIRO modelling systems required intensive computing power and so were run on CSIRO operated super computers named Ruby and Pearcey. Ruby is supercomputer with a large number of nodes, but few cores per node and is mostly used for data manipulation and storage. Pearcey has a large number of cores per node and is used for running highly parallelised tasks. The first two CCAM domains were run on Ruby, as they were low enough resolution for the number of cores per node to matter less for run time. The queue for Ruby was substantially shorter than the queue for Pearcey. The final CCAM domain had to be run on Pearcey due to the high resolution. CTM was run only on Ruby as the way in which it was parallelised couldn't take advantage of the high number of cores of Pearcey.

To run CCAM a number of scripts had to be created to first set up the input data for the domains, and then to run the model itself. Care had to be taken to ensure the parameters used were compatible with CTM. The same was true of CTM however a larger number of scripts were used due to CTM requiring more inputs such as fire sources, road sources and shipping sources. This is because CTM simulates a large number of different chemicals and aerosol modes, requiring initial and boundary conditions.

Due to the complexity, the CTM runs ran into many problems and only a single day run was completed using the first two domains. This was even without some of the inputs such as shipping that would have been required to produce meaningful results. The preliminary run of CTM for a single day was however enough to show that the CCAM runs had been performed correctly for use with CTM.

7.2.4 Comparison Data

To try and measure the accuracy of the output from CCAM measurement data was needed for comparison. The Australian Government's BOM collects such data and makes it available through its Climate Data Online tool (Meteorology, 2013). The data is sorted by stations, of which there are hundreds all around Australia. Each station collects a number of different measurements such as temperature, wind speed,

rainfall, humidity, pressure and so on. Not every station has the same measuring equipment and so some stations have no data for some measurements.

A number of station locations were selected to extract data from (see figure 7.8). They were chosen for their location within the final CCAM domain (see figure 7.6) and for their locality along the coastline and within the GBR as this was the region of focus. A script was written to extract the data in a form that was usable for comparison with the CCAM data.

Table 7.5: *The list of BOM locations that the CCAM output was compared to.*

Station Number	Station Name	Latitude	Longitude
200283	Willis Island	-16.2878	149.9652
031037	Low Isles	-16.3842	145.5592
200879	Arlington Reef	-16.7226	146.1124
200880	Lihou Reef	-17.133	152.145
032141	Lucinda Point	-18.5203	146.3861
033106	Hamilton Island	-20.3658	148.9536
033119	Mackay	-21.1172	149.2169
200001	Middle Percy Island	-21.6628	150.2711
033294	Yeppoon	-23.1364	150.7506
039122	Heron Island	-23.4417	151.9125
039322	Rundle Island	-23.5293	151.2763
039059	Lady Elliot Island	-24.1116	152.7161

To quantify the difference between the measurements and model data two parameters were calculated. The first was the mean of the residuals \bar{r} .

$$\bar{r} = \frac{1}{n} \sum_{i=1}^n (c_i - b_i). \quad (7.7)$$

Where n is the number of data points, generally 31 for each day of October, and b_i are the measurement data points collected from BOM. The CCAM data needed to be processed to extract a single value for each day, as the model output was hourly. Generally this took the form of finding the minimum or maximum value in the day to produce b_i . The mean residual provides direction and unit based scale of any differences.

The second quantifying parameter was the mean of percentage differences (MPD)

7.2. STUDY DESIGN

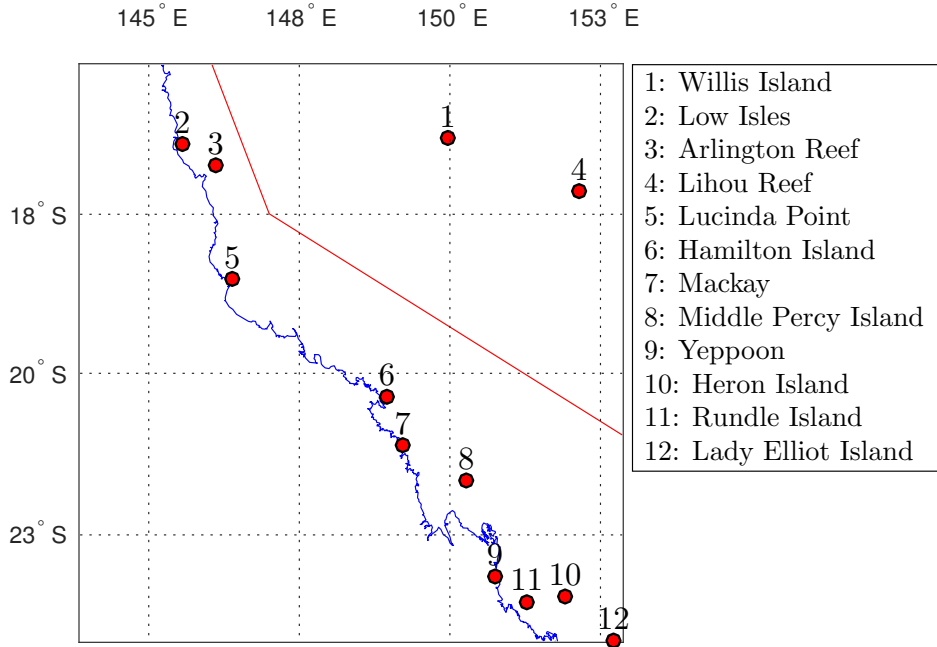


Figure 7.8: The locations of a number of BOM stations where data was taken from to compare with the results of the CCAM runs.

notated here as \overline{PD} .

$$\overline{PD} = \frac{1}{n} \sum_{i=1}^n \frac{|c_i - b_i|}{b_i}. \quad (7.8)$$

This uses the same variables as equation (7.7). The MPD uses the absolute value of the residuals to prevent cancellation if the individual residuals oscillate between positive and negative. It gives the magnitude of the difference, but normalised so that values from different sample locations can be compared. The standard deviation of the percentage differences was also calculated.

7.2.5 CCAM Data Reduction

The variables output by CCAM, such as temperature or wind speed, are assembled as a 4D matrix. Two dimensions are the latitude and longitude, indicating location. The third is as series of pressure levels, which substitute for height as air pressure decreases vertically. The fourth dimension is time. Plotting CCAM's output requires reduction of two of these dimensions.

To produce time series plots, the latitude and longitude dimensions need to be averaged. To do this either values across the entire map must be averaged, or a

region of interest must be extracted at each time step and averaged. To create maps of the data, each latitude and longitude point can be averaged over time. Either way, the pressure levels also need to be averaged, or a single level must be selected. It is also possible to average over the spatial and time dimension and create a pressure level plot.

7.2. STUDY DESIGN

8. Results

8.1 HYSPLIT Output

A very large number of back trajectories were modelled using HYSPLIT and transformed into interpolated histogram maps using the technique described in section 7.1.1. This was done to find the best months and locations for collecting air that had travelled over the GBR (see section 7.2.1). Each following section describes an aspect of the selection process.

8.1.1 Year Long Back Trajectory Histograms

A series of back trajectory histograms for a single location (Lucinda Jetty) are shown in figure 8.2 with a plot for each month. These histograms are produced from four years of back trajectories, from 2011 to 2014. All months show a greater fraction of back trajectories coming off the ocean rather than from the land. The best months are those with the greatest majority of back trajectory points over the reef. This ensures that any DMS or its products, produced by the reef, are likely to end up at the modelled location. The figure 8.2 is a sample of 96 plots that were produced.

8.1. HYSPLIT OUTPUT

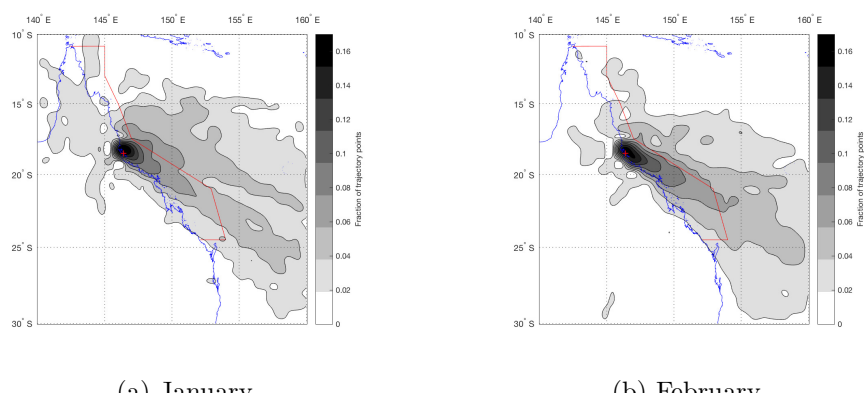


Figure 8.1: Continued...

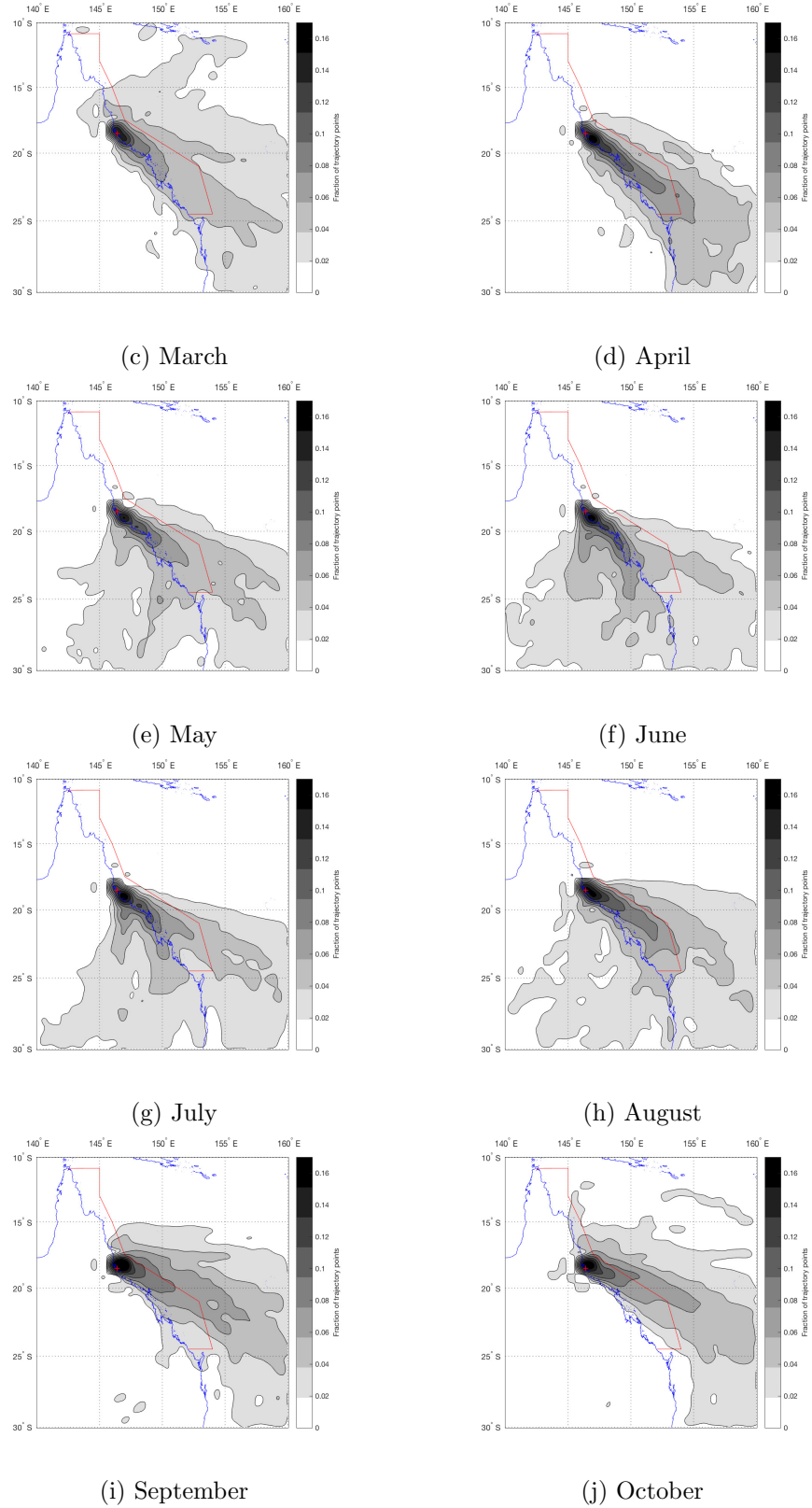


Figure 8.1: Continued...

8.1. HYSPLIT OUTPUT

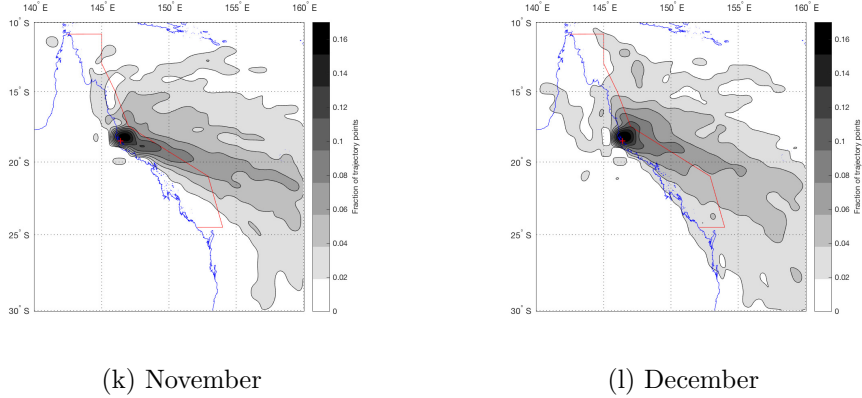


Figure 8.1: Interpolated histograms of back trajectory points modelled six times daily, for the months labelled, over the years 2011 to 2014, at Lucinda Jetty -18.520, 146.386.

8.1.2 Coastal Location Back Trajectory Histograms for October

With guidance from the plots in figure 8.2 and several other groups of year based of plots based on the locations listed in table 7.1, the month of October was selected for further modelling and the experimental campaign. The full ensemble of HYSPLIT plots for the coast line locations for October were examined to try and identify sites for setting up equipment (see figure 8.2). Again, the best sites have the greatest proportion of back trajectory points over the GBR, especially where the reef is dense. A second factor for these coastal locations was anthropogenic sources of aerosols. Sites with less back trajectories coming from inland or along the coastline would likely contain less anthropogenic aerosols.

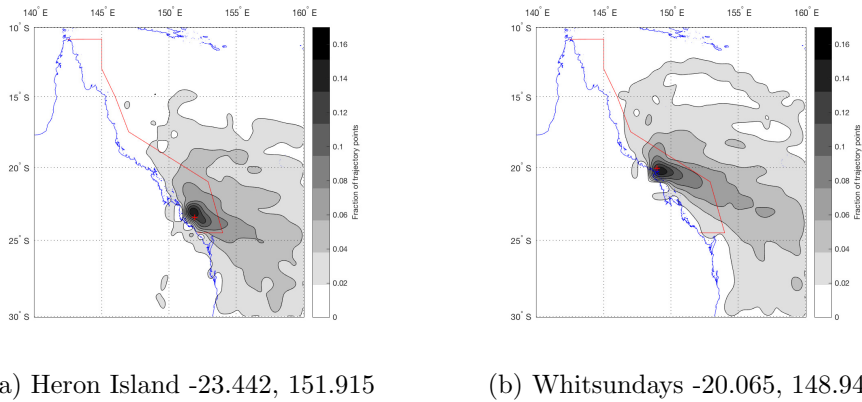


Figure 8.2: Continued...

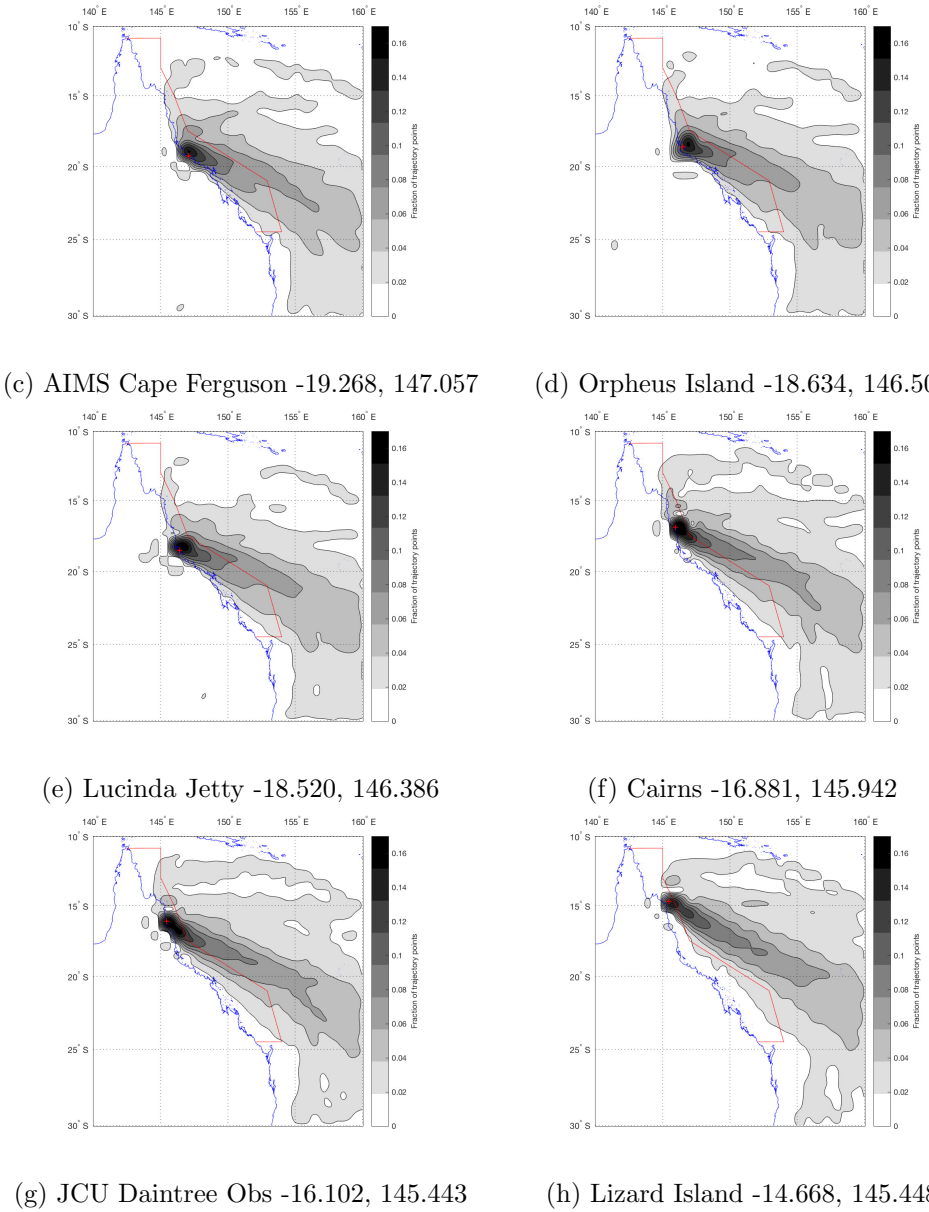


Figure 8.2: Interpolated histograms of back trajectory points modelled six times daily, during October, over the years 2011 to 2014 at the locations labelled.

8.1. HYSPLIT OUTPUT

8.1.3 Ship Location Back Trajectory Histograms for October

For the second part of the experimental campaign the ship would be sampling from in and around the reef. To help guide the selection of the path and stopping locations for the ship, a group of interpolated histogram plots were created using locations off the coast of Queensland (see table 7.2). The same criteria for selection used in section 8.1.1 was applied.

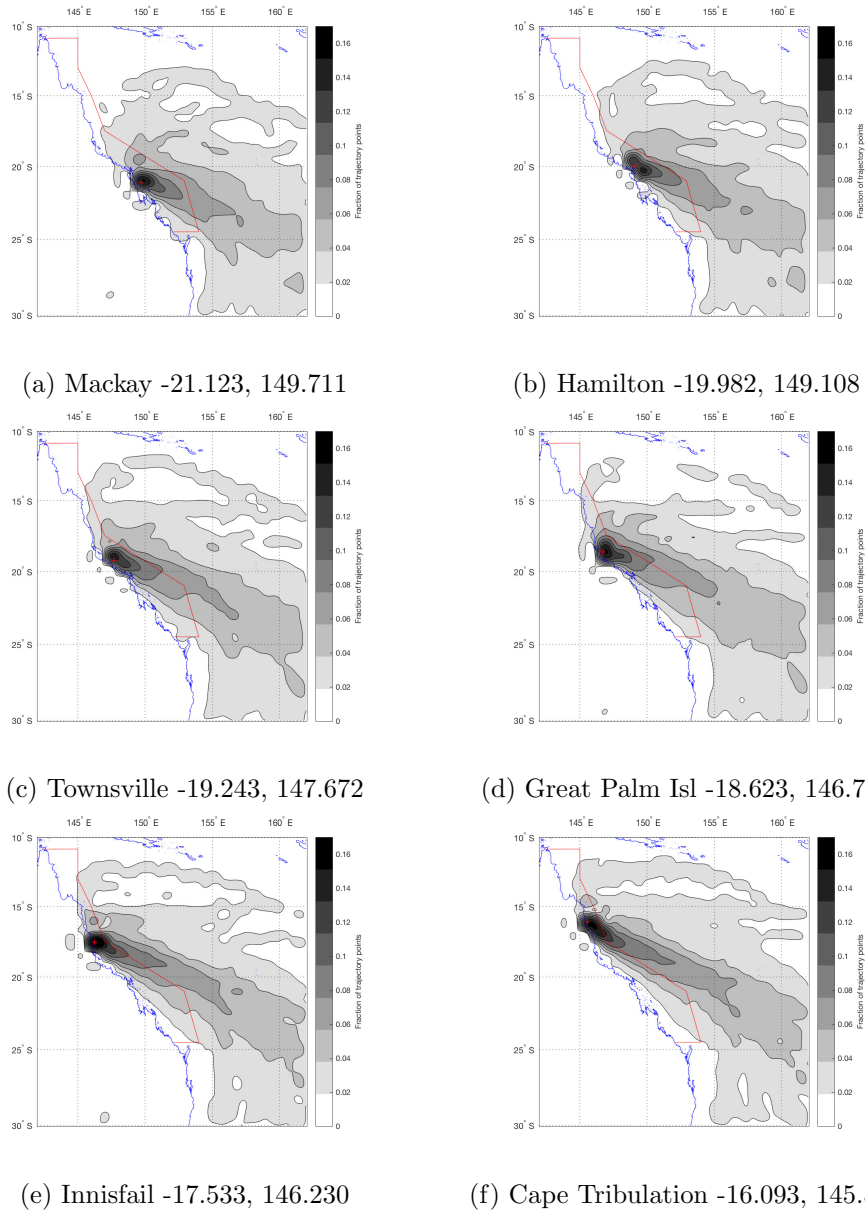


Figure 8.3: Interpolated histograms of back trajectory points modelled six times daily, during October, over the years 2011 to 2014 at the locations labelled.

8.2 CCAM Validation

The validity of CCAM's output is important for understanding the limitations of the model. Interpretation of the output should be modified by these limitations. Measurement data was retrieved from the BOM and then compared to data from the same locations in the CCAM output. The variables available were maximum air temperature, minimum air temperature and maximum wind speed. The locations of BOM stations used in this section can be found in table 7.5.

8.2.1 Mean Residuals

To find out if there was a trend to the predictions of CCAM the mean residuals were calculated. Subtracting the CCAM data from the available BOM data and then averaging these residuals for each location produced the values in table 8.1. The sign of these values indicates the trend of the model, whether it over (+ve) or under (-ve) predicts the variable in question at that location. They also provide the scale in the units of the measurement.

Table 8.1: *The mean residuals from a comparison of CCAM data with BOM data sampled from a series of Queensland locations.*

Station Name	Max Temp Mean Residuals (°C)	Min Temp Mean Residuals (°C)	Max Wind Speed Mean Residuals (m/s)
Willis Island	-1.61	1.35	-3.28
Low Isles	-2.69	1.88	-3.01
Arlington Reef	-	-	-3.15
Lihou Reef	0.70	0.95	-2.84
Lucinda Point	0.01	2.06	-2.55
Hamilton Island	-0.53	1.65	-8.02
Mackay	-2.51	2.19	-2.80
Middle Percy Island	-0.78	2.78	-5.02
Yepoon	-0.87	2.15	-4.25
Heron Island	-	-	-2.27
Rundle Island	-0.81	1.40	-2.85
Lady Elliot Island	-2.69	1.57	-2.40

8.2. CCAM VALIDATION

8.2.2 Comparison of BOM and CCAM Data

The percentage difference between the CCAM and BOM values were calculated for the available variables and station locations. Taking the mean of these percentage differences over time for each location provides an indicator for how well CCAM is simulating the interactions surrounding these atmospheric properties. These MPD values measure the normalised distance allowing comparison with each other.

Table 8.2: *The Mean Percentage Differences, calculated from a comparison of CCAM data with BOM data, sampled from a series of Queensland locations.*

Station Name	Max Temp Mean Percentage Difference	Min Temp Mean Percentage Difference	Max Wind Speed Mean Percentage Difference
Willis Island	5.74 ± 2.41	6.64 ± 4.86	23.3 ± 9.8
Low Isles	9.16 ± 3.15	8.44 ± 4.34	22.8 ± 10.0
Arlington Reef	-	-	22.7 ± 11.4
Lihou Reef	3.08 ± 1.35	5.54 ± 3.76	21.5 ± 11.0
Lucinda Point	2.77 ± 1.95	9.74 ± 5.87	20.8 ± 11.0
Hamilton Island	2.83 ± 1.92	7.91 ± 4.56	55.9 ± 6.5
Mackay	8.92 ± 2.56	13.0 ± 9.89	26.7 ± 11.2
Middle Percy Island	3.26 ± 1.90	14.0 ± 4.20	38.6 ± 11.4
Yeppoon	3.87 ± 1.91	12.0 ± 10.2	36.8 ± 7.7
Heron Island	-	-	21.7 ± 9.1
Rundle Island	3.81 ± 3.88	6.76 ± 3.19	22.7 ± 10.0
Lady Elliot Island	10.2 ± 2.6	7.93 ± 5.30	21.1 ± 10.0

The most direct way of comparing the BOM and CCAM data is to plot them against each other, over time. A comparison of the shapes of the graphs can be made along with their distance from each other. Spikes and noise are also obvious. The locations with the highest and lowest MPDs, for each measurement, were chosen as a sample from table 8.2. They show where the values in table 8.2 and section 8.2.1 came from and how much variation there is between locations.

CHAPTER 8. RESULTS

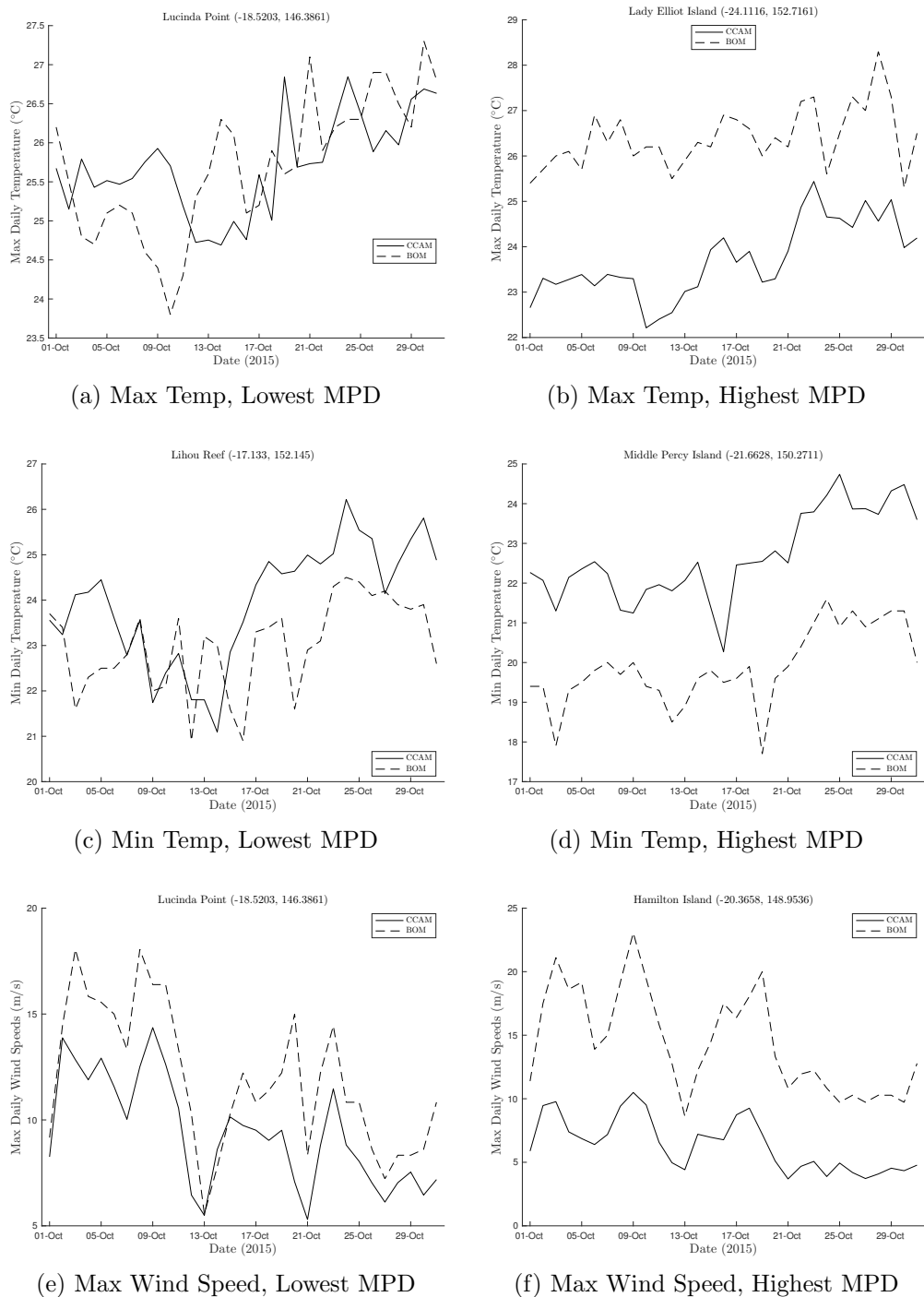


Figure 8.4: A comparison of BOM station data and data produced by CCAM. Locations were selected based on the lowest (left) and highest (right) mean of percentage differences between the two data sets (taken from table 8.2). The variables are the Maximum and Minimum daily Air Temperatures near the surface, and the Maximum daily 10 m Wind Speed.

8.3 CCAM Output

As discussed in section 7.2.5 the output from CCAM must be reduced to be able to plot it. The region of interest was chosen as the GBR for collapsing the spatial dimensions. The points within it were extracted and averaged for each hour in the model. To produce the maps, the hourly values of the time dimension, for each point in the map, were averaged and these points were gridded onto the final CCAM domain.

Each of the variables examined in this section explore the output of CCAM. There is a particular focus on parameters of the atmosphere that influence DMS production, its movement and transformation, and its potential for effecting cloud coverage and rain.

8.3.1 Surface and Pressure Level Heights

As CCAM uses pressure Levels rather than height for its vertical axis, seeing the relationship between the pressure Levels and the geopotential height is important for drawing conclusions requiring the actual height. This relationship can be seen in figure 8.5. The height of the surface is also important as it shows the location of surface artefacts like mountain ranges (see figure 8.6).

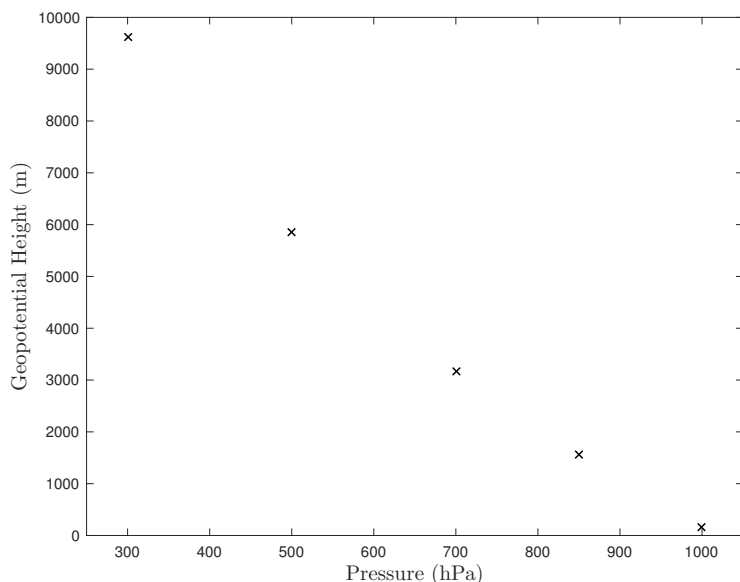


Figure 8.5: The Geopotential Height averaged from all points within the GBR and also averaged over time then plotted against the modelled Pressure Levels.

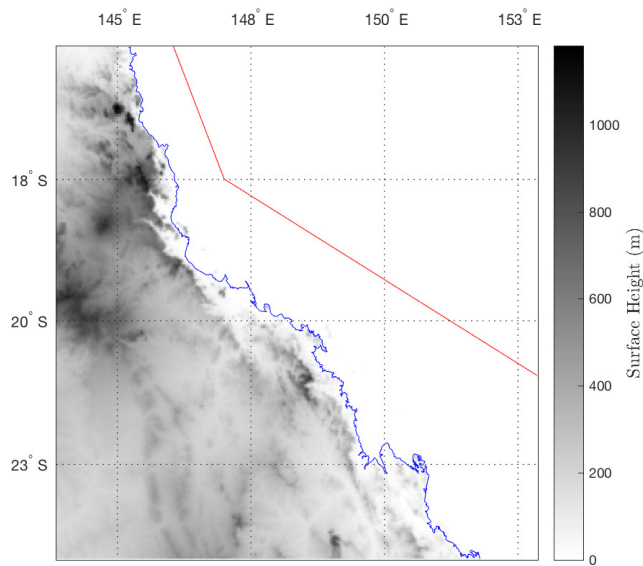


Figure 8.6: A map of the Height of the surface of the earth and ocean within the final CCAM domain.

8.3.2 Air and Surface Temperatures

There are a number of different levels that temperatures can be sampled from. The five outputted pressure levels, the bottom pressure level the model simulated, the screen level (1.5 m above the surface), and the surface temperature. These figures provide an image of what is happening with the air temperature within the simulated domain, over time, and how it varies vertically. The air temperature map in figure 8.7 contextualises the temperatures used in section 8.2.2. The temperature over time for the GBR in figure 8.9 points to weather phenomena occurring during this month.

8.3. CCAM OUTPUT

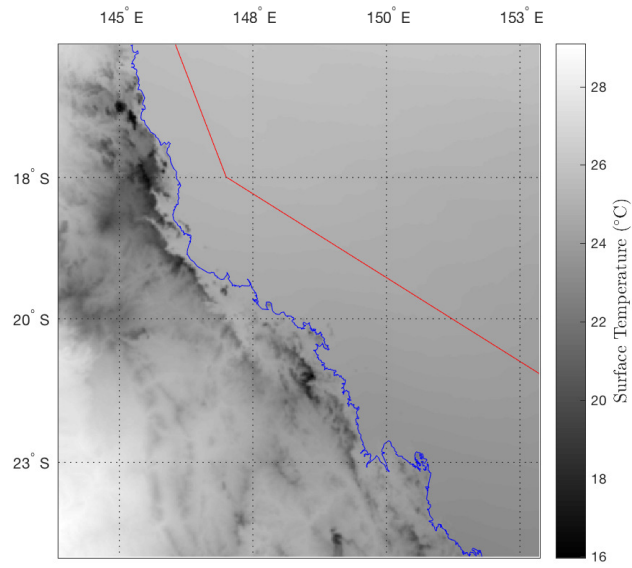


Figure 8.7: A map of the Air Temperature at the lowest simulated Pressure level. The Temperatures were averaged over the modelled month, October 2015.

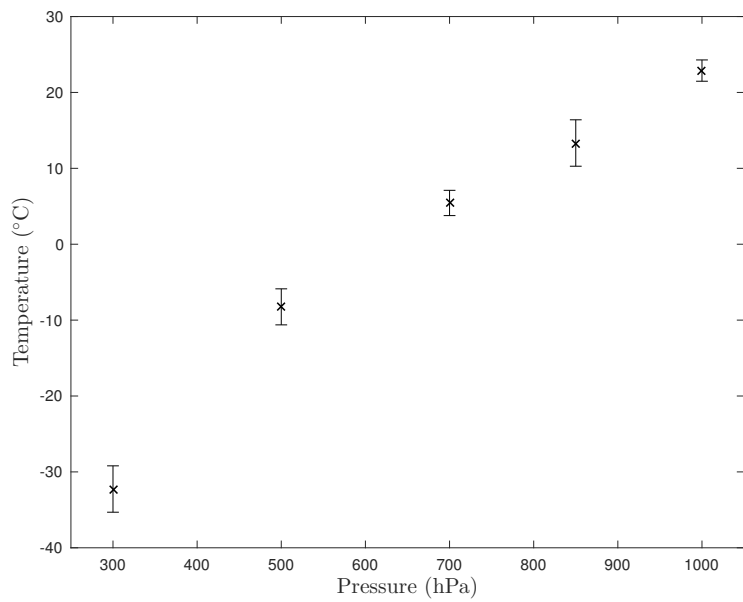


Figure 8.8: The Air Temperature averaged from all points within the GBR and also averaged over time then plotted against the modelled Pressure Levels.

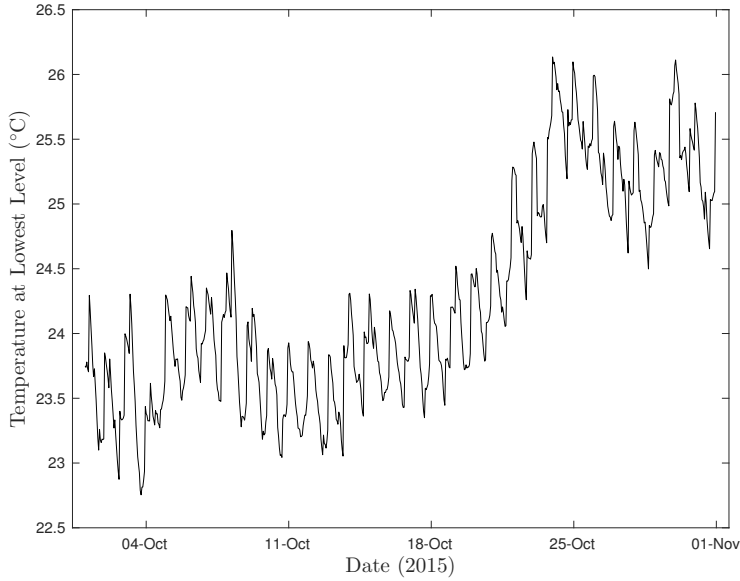


Figure 8.9: The Air Temperature at the lowest simulated Pressure level, averaged from the points inside the GBR region of the final CCAM domain.

8.3.3 Wind Directions and Speed

The wind in this system causes two of the main effects being examined. The first is the speed of the wind across the surface of the ocean as this is the largest influencing factor of DMS surface flux (see section 6.2). The second is in which direction and how far the DMS and its products are moved. These two points are illustrated in figure 8.11 and figure 8.10 respectively.

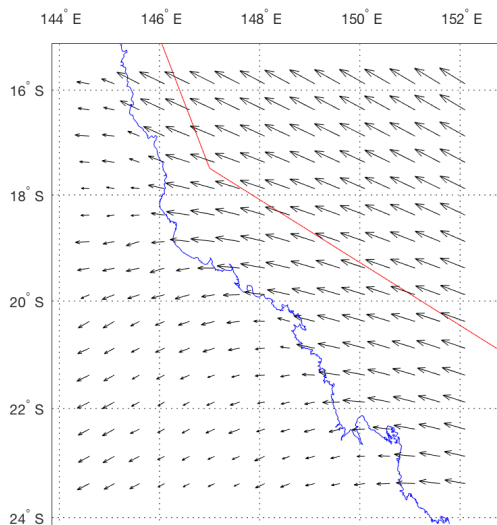


Figure 8.10: A map of the final CCAM domain showing the modelled 10 metre Wind vectors.

8.3. CCAM OUTPUT

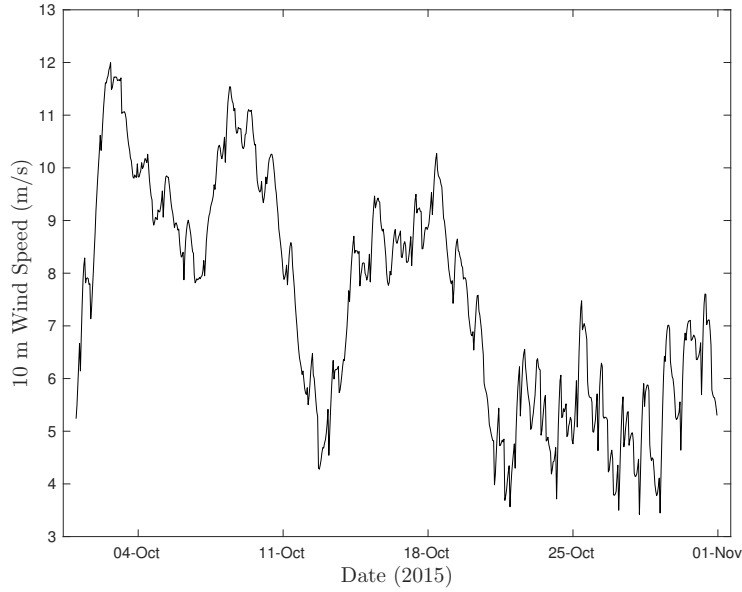


Figure 8.11: The magnitude of the 10 metre Wind Speed, averaged from the points inside the GBR region of the final CCAM domain.

8.3.4 Clouds, Rain and Radiation

CCAM simulates three levels of cloud coverage as low, mid, and high cloud fraction. Combining these gives the total cloud fraction. The cloud coverage effects the amount of radiation hitting the surface of the earth. The radiation flux at the surface of the earth is composed of a number of source, direct, diffuse, reflected, and produced. Cloud coverage alters the fraction of direct and diffuse radiation. The net radiation at the surface of the GBR can be see in figure 8.13. The cloud coverage also effects the presence of rain. In figure 8.15 and in figure 8.14 the rain fraction and total cloud fraction can be seen mapped to the modelled domain. This shows their distribution across the GBR, but also along the Queensland coast.

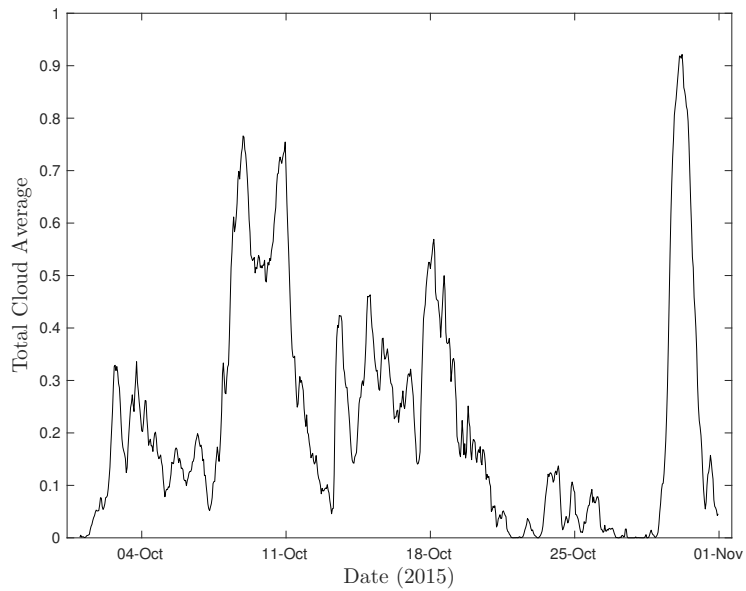


Figure 8.12: The Total Cloud Fraction, averaged from the points inside the GBR region of the final CCAM domain.

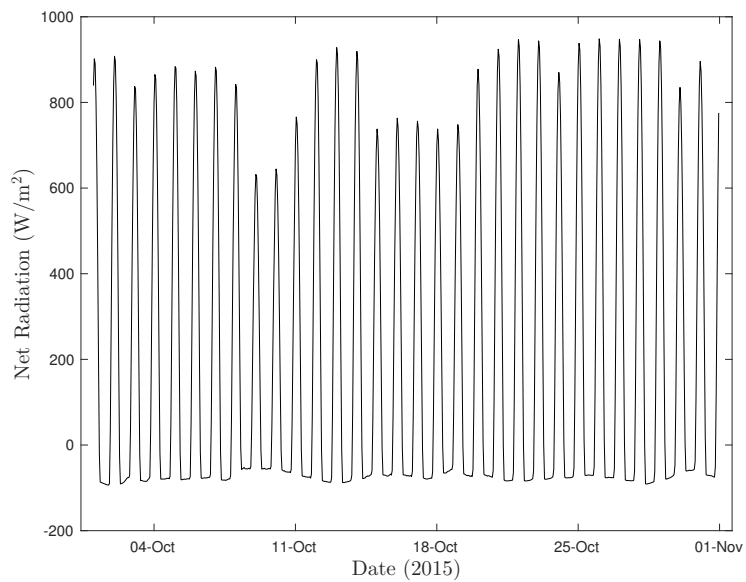


Figure 8.13: The Net Radiation striking the surface, averaged from the points inside the GBR region of the final CCAM domain.

8.3. CCAM OUTPUT

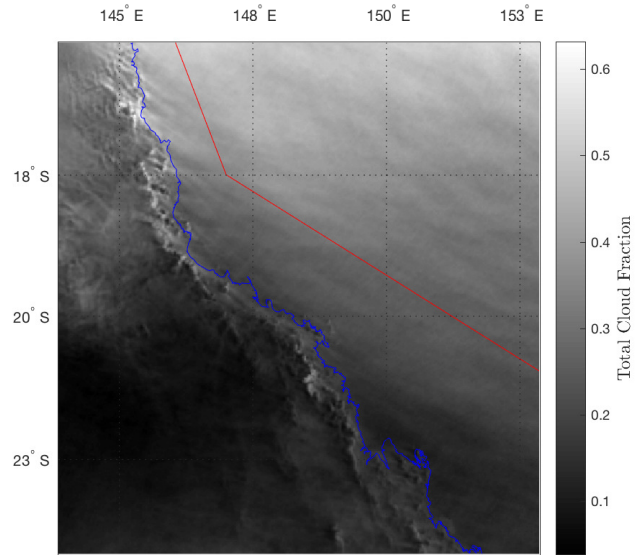


Figure 8.14: A map of the Total Cloud Fraction consisting of the Cloud Fractions from all levels. The Total Cloud fractions were averaged over the modelled month, October 2015.

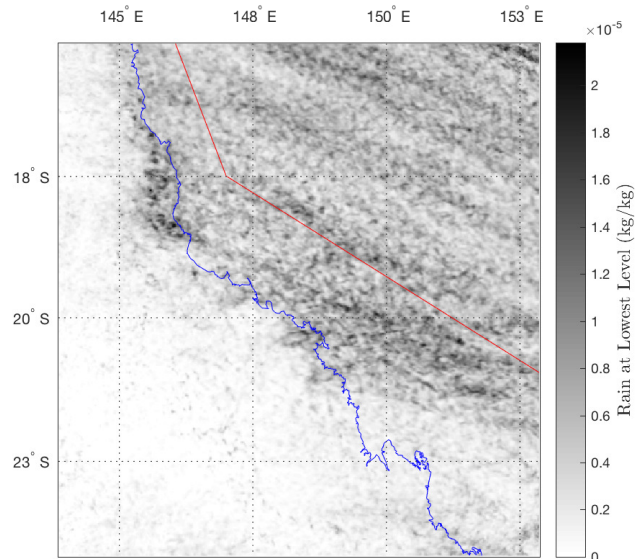


Figure 8.15: A map of the Rain fraction at the 1000 hPa level of the model. The Rain fractions were averaged over the modelled month, October 2015.

9. Analysis and Discussion

9.1 HYSPLIT Modelling

9.1.1 Assessing Locations and Months

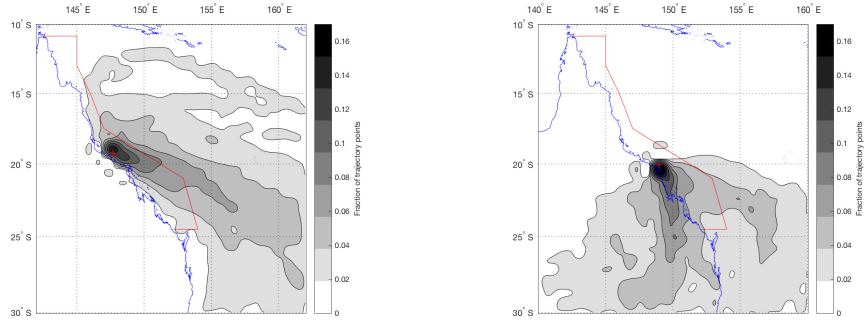
The interpolated histograms in section 8.1 show a general trend of air packets coming from the Pacific Ocean and towards the coast. The direction of wind vectors in figure 8.10, modelled in CCAM agrees, with a majority pointing in the westerly direction. This indicates that almost year round, at locations along the Queensland coast, the majority of the air packets that arrive there have passed over the GBR. There are identifiable differences between locations and months that determine suitability for coastal experimental locations and ship routes.

Looking at figure 4.1, the reef runs right down the Queensland coast, but the coast begins to jut out to the east at around 20° S. This creates a section of the reef running more to the east-southeast, matching the wind direction. The reef also widens into the Swain Reefs creating a larger body. Selecting locations and months where the interpolated histograms show a large proportion of air packets coming over that stretch of reef provides the highest chance of detecting the reefs output of DMS. It is also important that as little as possible originates from the land, as anthropogenic sources would mask the reef sources. In figure 9.1 there are examples of this analysis for selecting suitable and unsuitable locations and months.

9.1.2 Advising the Experimental Campaign

The best months appeared to occur in the later part of the year, September, October, and November. This was fairly consistent across all locations. October was the month selected for the experimental campaign, based on ship availability and this analysis. One of the coastal locations chosen was Mission Beach (-17.87 146.11). The

9.1. HYSPLIT MODELLING



(a) October, Townsville -19.24, 147.67 (b) June, Whitsundays -20.06, 148.95

Figure 9.1: A comparison of interpolated histograms of back trajectory points modelled six times daily, over the years 2011 to 2014. The locations and months are listed. An example of a suitable location and month, with the majority of the air travelling over a large section of the GBR can be seen in figure 9.1a. Figure 9.1b is an example of an unsuitable location, with the bulk source coming off the land.

location modelled in figure 9.2 is very close to this and shows a decent proportion of air packets coming off the reef, with little influence from the land.

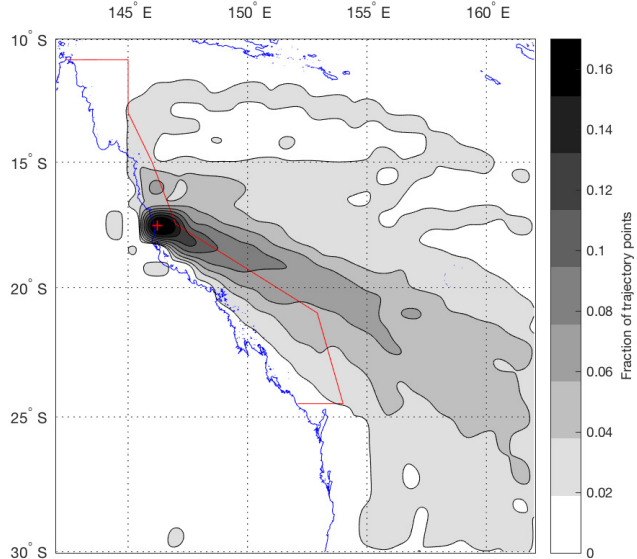


Figure 9.2: Interpolated histograms of back trajectory points modelled six times daily, during October, over the years 2011 to 2014 at Innisfail (-17.533, 146.230). This is an example of a suitable location that was used in the campaign.

9.2 CCAM Modelling

9.2.1 Modelling of Meteorology Processes

While CCAM doesn't model aerosols, and thus CCN, it still produces cloud and rain data by assuming their presence. Humidity, pressure and temperature are used for generating cloud fractions. In figure 8.14 and figure 8.15 there are high levels of both total cloud fraction and rain along the Queensland coastline. Looking at the map of the surface height figure 8.6 the same areas are low, almost sea level height regions, abutted by mountains. Moist warm air from the ocean moves inland and is pushed upwards by the increasing surface height. This cools the air without changing its water content causing condensation to occur (see section 2.2).

The HYSPLIT work showed that most of the air coming from the Pacific Ocean to the coast. In figure 9.3 the bottom pressure levels (highest values) show the east-west wind speed for most of the month as a negative value indicating an easterly wind (travelling towards the west). These easterly winds are the trade winds caused by a combination of the Hadley cell circulation and the Coriolis force (Seinfeld et al., 2012, Chapter 1). The high, positive east-west wind speeds at the top pressure level is likely the top of the Hadley cell.

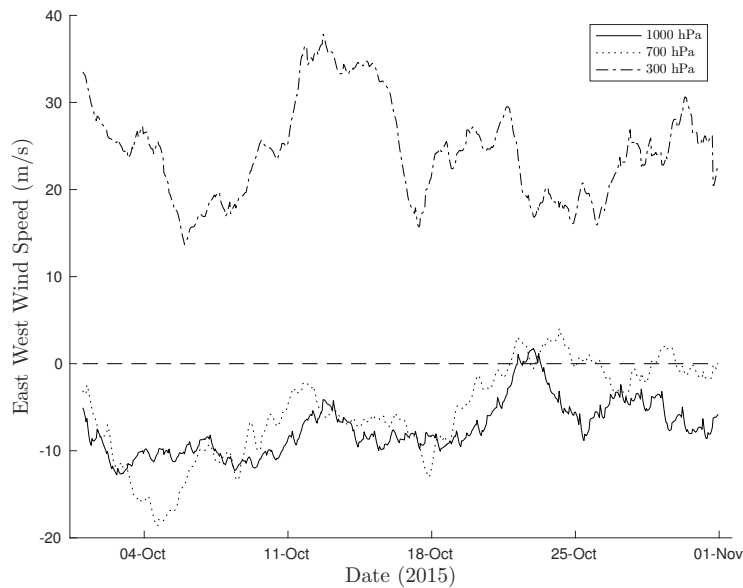


Figure 9.3: The east-west Wind Speed, averaged from the points inside the GBR region of the final CCAM domain. The highest, middle, and lowest pressure levels are shown.

An interesting meteorological event occurs over the GBR towards the end of the

9.2. CCAM MODELLING

month beginning on the 19th. This can be seen in figure 8.11 where the magnitude of the wind decreases from an average of 8.77 m/s to an average of 5.55 m/s. The opposite occurs to the temperature at the bottom pressure level (see figure 8.9), with an average of 23.72 °C before the 19th rising to an average 25.10 °C after the 19th. The cause of this shift is likely due to a pressure front moving through the GBR. In figure 9.4 the mean sea level pressure can be seen dropping down to 1014 hPa from 1019 hPa. Winds move towards low pressure regions (Seinfeld et al., 2012). The low moves from west to east across the GBR over the last part of the month countering the trade winds, decreasing the wind speed. This in turn increases the temperature over the GBR as the winds transfer less of the solar heating of the reef away.

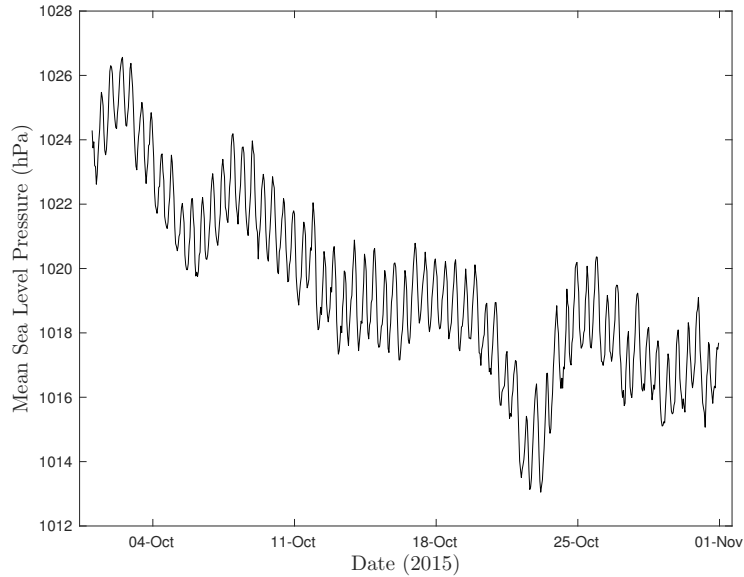


Figure 9.4: The Mean Sea Level Pressure, averaged from the points inside the GBR region of the final CCAM domain.

9.2.2 Influences on DMS Production

Both ocean temperatures and solar radiation levels effect the production of DMSP by corals (Raina et al., 2013), (Fischer et al., 2012). In figure 9.5 the surface temperature of the GBR is plotted over time with an increase of 1 °C towards the end of the month. The plots in figure 8.12 and figure 8.13 show a link between the amount of total surface radiation to total cloud fraction. This highlights the importance of local meteorology on surface temperature, and total surface radiation, the main influences on DMS production.

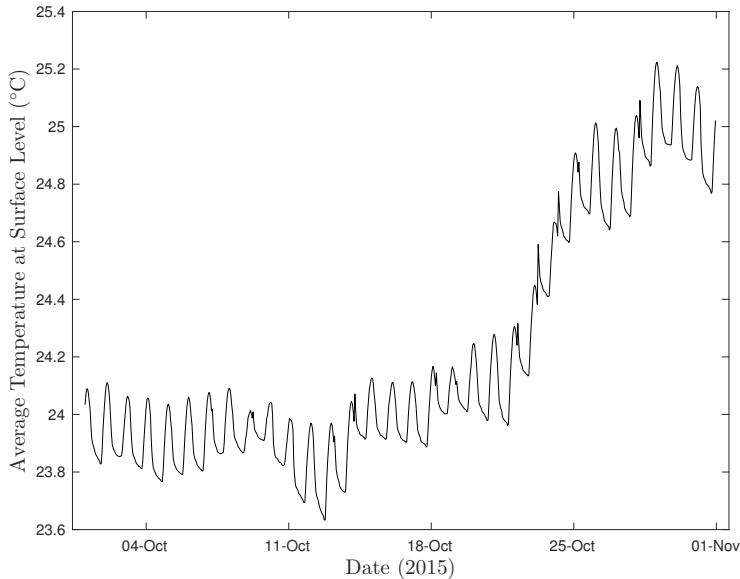


Figure 9.5: The Surface Temperature, averaged from the points inside the GBR region of the final CCAM domain.

In figure 8.11 the wind speed across the modelled region of the GBR can be seen varying between 3.5 m/s and 12 m/s. The wind speed varies quite drastically over the month with the last third of the month experiencing a prolonged decrease. The transfer of DMS from the ocean into the air depends heavily on the wind sheer at the surface (see section 6.2) (A. J. Kettle et al., 2000). This indicates that the bulk of DMS moving into the atmosphere would also experience these fluctuations making it advisable to use a DMS surface flux model based on CCAM's wind speed rather than directly feeding in DMS atmospheric concentrations.

9.2. CCAM MODELLLING

9.2.3 Limitations and Reliability of CCAM Data

The percentage difference was calculated between the CCAM and BOM values for the available variables and station locations. Taking the mean of these percentage differences over time (see equation (7.8)) for each location provides an indicator for how well CCAM is simulating the interactions surrounding these atmospheric properties. These values measure the normalised distance allowing comparison with each other.

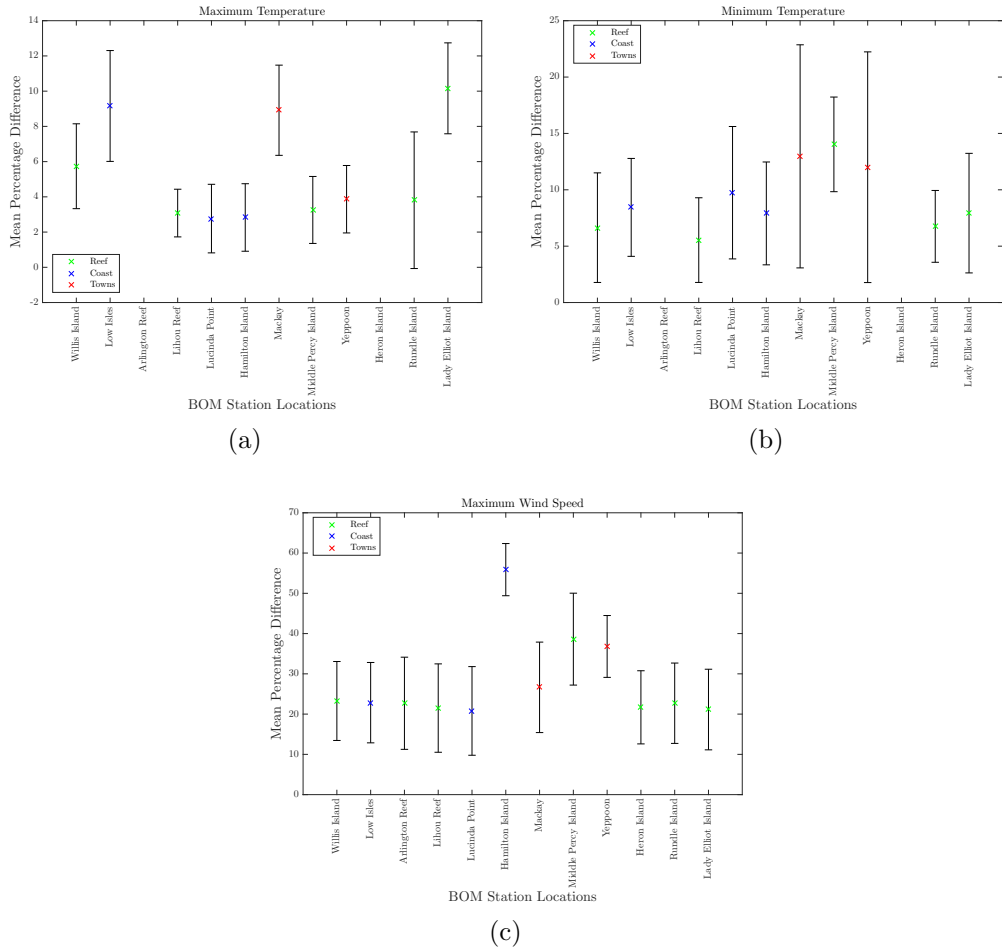


Figure 9.6: The mean percentage differences and their standard deviations calculated by comparing the labelled measurement variables at a number of BOM station locations with the output of CCAM.

Looking at the values in table 8.1, the modelled temperature appears to be underestimating the maximum temperature and overestimating the minimum temperature. This may be a lack of variation in the model, however in figure 9.6 the trend is fairly constant across the month. A similar problem effects wind speeds with CCAM under estimating the maximum wind speed. The mean percentage difference for maximum

wind speed is quite high, around 20 %. While the mean percentage difference for both temperatures is lower, this must be factored into any further modelling done using the CCAM data.

9.2. CCAM MODELLING

10. Conclusion

10.1 Future Research

The next step is to use the CCAM modelling runs to run CTM and GLOMAP. However, there are a number of precautions that need to be taken.

The analysis of current chemistry relating to DMS and its products in section 3.1 reveal a complex system. Ensuring that the chemical reactions are treated with respect to current theory should improve predictions. In section 3.2.2 the different ways in which DMS is prevented from eventually forming CCN was summarised. These mechanisms will need to be incorporated into the operation of both CTM and GLOMAP-mode.

DMS surface flux values are required to provide input into CTM. Changing ocean surface temperatures and wind speeds alter this flux through the mechanisms outlined in section 6.2. A surface flux model, potentially taking meteorological data from CCAM will need to be developed. This model should take into account wind speed, surface temperature and net surface radiation. It may be possible to alter the surface flux model, or change the setup for CCAM, to simulate a number of different scenarios resulting from changes in climate and changes in coral cover.

Once a complete run of the three models has been completed for October 2015, the modelling system should be cycled again for October 2016. Once the experimental campaign has completed and data has been extracted, the modelling data should be compared against the experimental data.

10.2 Closing Remarks

In this thesis the existing research surrounding DMS, and its effects on CCN production, were examined. The focus was on modelling the system for the GBR region.

10.2. CLOSING REMARKS

Investigating the atmosphere, its many layers, and the aerosols in it established the underlying theory for CCN, and for atmospheric modelling. Reviewing the chemistry and role of DMS, and coral's production of it in the GBR, identified the requirements for modelling chemical transport and the creation of new particles. The models to be used were examined for their function and viability. Finally the climatology of DMS was researched and methods for developing maps of DMS surface flux were found. The literature indicates that there is a necessity for localised models of the GBR's effect on cloud cover that existing research has not covered.

Modelling in HYSPLIT was performed to guide selection of experimental locations along the Queensland coastline. A modelling system was organised for regional modelling work in the GBR and Queensland coast regions. The atmospheric part of the modelling system, CCAM, was run for the month of October, the month selected for the experimental campaign. The CCAM data was analysed and compared with measurement data from BOM.

The HYSPLIT work showed that the majority of the air arriving along the Queensland coast came from across the GBR. A month, October, was chosen guided partly by the HYSPLIT work. Locations for data collection were also chosen along with a path and stopping points of a ship voyage.

The CCAM data mirrored the HYSPLIT work, showing that the prevailing winds were the trade winds providing GBR sourced air to the coast for the majority of October. The data also indicated a low pressure system moving across the GBR effecting surface temperatures and wind speeds across the GBR. This highlights the importance of regional atmospheric modelling for modelling DMS production by the reef and its flux into the atmosphere.

The atmospheric conditions for the formation of clouds along the Queensland coastline are present in the CCAM model. The air in which these clouds are formed is almost certainly coming from across the GBR. This fulfils some of the requirements for the GBR influencing rainfall over the eastern part of Queensland.

A comparison between BOM measurement data and the CCAM data was performed. The results showed an underestimation by CCAM of the range of temperatures experienced at the BOM stations. The maximum wind speed was also underestimated by CCAM. These results have been forwarded to the team working on the CCAM model.

What remains is whether DMS production is high enough, the chemical pathway from DMS to CCN actually functions, the quantity of CCN produced isn't swamped by other sources, and whether the pathway can occur fast enough before the air

CHAPTER 10. CONCLUSION

mass has moved over the coastline.

10.2. CLOSING REMARKS

Bibliography

- Ayers, G P and Gras, J L (1991). “Seasonal relationship between cloud condensation nuclei and aerosol methanesulphonate in marine air”. In: *Nature* 353.6347, pp. 834–835 (cit. on pp. 19, 20).
- Bandy, Alan et al. (2011). “Pacific Atmospheric Sulfur Experiment (PASE): dynamics and chemistry of the south Pacific tropical trade wind regime”. In: *Journal of atmospheric chemistry* 68.1, pp. 5–25 (cit. on p. 31).
- Barnes, I, Hjorth, J, and Mihalopoulos, N (2006). “Dimethyl sulfide and dimethyl sulfoxide and their oxidation in the atmosphere”. In: *Chemical Reviews* 106.3, pp. 940–975 (cit. on pp. 2, 15–17, 42).
- Bigg, E Keith (2007). “Sources, nature and influence on climate of marine airborne particles”. In: *Environmental Chemistry* 4.3, pp. 155–7 (cit. on p. 13).
- Borthwick, David, Belcher, Barbara, and Hutson, Jonathan (2006). “Review of the Great Barrier Reef Marine Park Act 1975”. In: *Department of the Environment and Heritage*, pp. 1–222 (cit. on pp. 23, 24).
- Broadbent, Andrew D and Jones, Graham B (2004). “DMS and DMSP in mucus ropes, coral mucus, surface films and sediment pore waters from coral reefs in the Great Barrier Reef”. In: *Marine and Freshwater Research* 55.8, pp. 849–855 (cit. on p. 25).
- Cainey, Jill M, Sievering, Herman, and Ayers, Greg P (2007). “Where to now? A synthesis of current views of the CLAW hypothesis”. In: *Environmental Chemistry* 4.6, pp. 406–4 (cit. on pp. v, 1, 3, 20, 21, 26).
- Challa, Venkata Srinivas et al. (2008). “Sensitivity of atmospheric dispersion simulations by HYSPLIT to the meteorological predictions from a meso-scale model”. In: *Environmental fluid mechanics* 8.4, pp. 367–387 (cit. on p. 38).
- Charlson, Robert J et al. (1987). “Oceanic phytoplankton, atmospheric sulphur, cloud albedo and climate”. In: *Nature* 326.6114, pp. 655–661 (cit. on pp. v, 1, 15, 17–20).

BIBLIOGRAPHY

- Clarke, AD et al. (1998). “Particle production in the remote marine atmosphere: Cloud outflow and subsidence during ACE 1”. In: *Journal of Geophysical Research: Atmospheres (1984–2012)* 103.D13, pp. 16397–16409 (cit. on p. 20).
- Cope, Martin et al. (2009). *Chemical Transport Model - Technical Description*. CSIRO. The Centre for Australian Weather and Climate Research (cit. on pp. 3, 27, 41).
- Cope, Martin et al. (2014). *Sydney Particle Study*. CSIRO. The Centre for Australian Weather and Climate Research (cit. on pp. 28, 29, 41, 42).
- Draxler, R R and Hess, G D (1997). *Description of the HYSPLIT4 modeling system*. Tech. rep. (cit. on pp. 27, 38).
- (1998). “An overview of the HYSPLIT4 modelling system for trajectories”. In: *Australian meteorological magazine* (cit. on pp. 28, 38).
- Fischer, Esther and Jones, Graham (2012). “Atmospheric dimethylsulphide production from corals in the Great Barrier Reef and links to solar radiation, climate and coral bleaching”. In: *Biogeochemistry* 110.1-3, pp. 31–46 (cit. on pp. v, 3, 13, 73).
- Hoegh-Guldberg, Ove (1999). “Climate change, coral bleaching and the future of the world’s coral reefs”. In: *Marine and freshwater research* 50.8, pp. 839–866 (cit. on pp. v, 2, 3, 23).
- Hurley, Peter (1994). “PARTPUFF—a Lagrangian particle-puff approach for plume dispersion modeling applications”. In: *Journal of Applied Meteorology* 33.2, pp. 285–294 (cit. on p. 38).
- (2002). “The Air Pollution Model (TAPM) Version 2. Part 1: Technical Description”. In: *Technical Paper* 71 (cit. on pp. 27, 39).
- IPCC (2015). “Summary for Policymakers”. In: *Climate Change 2014 Mitigation of Climate Change*. Cambridge: Cambridge University Press, pp. 1–30 (cit. on pp. 1, 2, 10, 12).
- Jacob, Daniel J (2000). “Heterogeneous chemistry and tropospheric ozone”. In: *Atmospheric Environment* 34.12, pp. 2131–2159 (cit. on p. 17).
- Jacobson, Mark Z (2005). *Fundamentals of atmospheric modeling*. Cambridge university press (cit. on p. 27).
- Jones, Graham B and Trevena, Anne J (2005). “The influence of coral reefs on atmospheric dimethylsulphide over the Great Barrier Reef, Coral Sea, Gulf of Papua and Solomon and Bismarck Seas”. In: *Marine and freshwater research* 56.1, p. 85 (cit. on pp. 3, 4, 25, 26, 33).
- Jones, Graham et al. (2007). “Factors affecting the cycling of dimethylsulfide and dimethylsulfoniopropionate in coral reef waters of the Great Barrier Reef”. In: *Environmental Chemistry* 4.5, pp. 310–322 (cit. on pp. 23, 25).

BIBLIOGRAPHY

- Kettle, A J and Andreae, M O (2000). “Flux of dimethylsulfide from the oceans: A comparison of updated data sets and flux models”. In: *Journal of Geophysical Research* (cit. on pp. 32, 33, 73).
- Kettle, A J et al. (1999). “A global database of sea surface dimethylsulfide (DMS) measurements and a procedure to predict sea surface DMS as a function of latitude, longitude, and month”. In: *Global Biogeochemical Cycles* 13.2, pp. 399–444 (cit. on p. 33).
- Köhler, Hilding (1936). “The nucleus in and the growth of hygroscopic droplets”. In: *Transactions of the Faraday Society* 32, pp. 1152–10 (cit. on p. 13).
- Laing, A and Evans, JL (2011). *Introduction to Tropical Meteorology*. 2nd ed. The COMET Program (cit. on pp. 7–9).
- Lana, Arancha et al. (2011). “An updated climatology of surface dimethylsulfide concentrations and emission fluxes in the global ocean”. In: *Global Biogeochemical Cycles* 25.1 (cit. on pp. 33, 34).
- Lashof, D A and Ahuja, D R (1990). “Relative contributions of greenhouse gas emissions to global warming”. In: *Nature* 344, pp. 529–531 (cit. on p. 10).
- Leahy, Susannah M, Kingsford, Michael J, and Steinberg, Craig R (2013). “Do Clouds Save the Great Barrier Reef? Satellite Imagery Elucidates the Cloud-SST Relationship at the Local Scale”. In: *PLoS ONE* 8.7, e70400 (cit. on pp. 3, 23).
- Lefebvre, Mario (2006). *Applied Probability and Statistics*. 1st ed. Springer (cit. on p. 39).
- Liss, Peter S (1983). “Gas Transfer: Experiments and Geochemical Implications”. In: *Air-Sea Exchange of Gases and Particles*. Dordrecht: Springer Netherlands, pp. 241–298 (cit. on pp. 26, 33).
- Mann, G W, Carslaw, K S, and Spracklen, D V (2010). “Description and evaluation of GLOMAP-mode: a modal global aerosol microphysics model for the UKCA composition-climate model”. In: *Geoscientific Model Development* 3.2, pp. 519–551 (cit. on pp. 27, 42, 43).
- McGregor, John L (2005). *C-CAM: Geometric aspects and dynamical formulation*. CSIRO Atmospheric Research. CSIRO Atmospheric Research (cit. on pp. 3, 39, 40).
- McGregor, John L and Dix, Martin R (2008). “An updated description of the conformal-cubic atmospheric model”. In: *High resolution numerical modelling of the atmosphere and ocean*. Springer, pp. 51–75 (cit. on pp. 27, 37, 39).
- Merikanto, J et al. (2009). “Impact of nucleation on global CCN”. In: *Atmospheric Chemistry and Physics Discussions* 9.3, pp. 8601–8616 (cit. on p. 12).
- Meteorology, Bureau of (2013). *Bureau of Meteorology Climate Data Online*. URL: <http://www.bom.gov.au/climate/data/> (visited on 10/20/2016) (cit. on p. 48).

BIBLIOGRAPHY

- O'Dowd, Colin D and Smith, Michael H (1993). "Physicochemical properties of aerosols over the northeast Atlantic: Evidence for wind-speed-related submicron sea-salt aerosol production". In: *Journal of Geophysical Research: Atmospheres (1984–2012)* 98.D1, pp. 1137–1149 (cit. on p. 19).
- O'Dowd, Colin D et al. (1997). "Marine aerosol, sea-salt, and the marine sulphur cycle: A short review". In: *Atmospheric Environment* 31.1, pp. 73–80 (cit. on p. 15).
- O'Dowd, Colin D et al. (2004). "Biogenically driven organic contribution to marine aerosol". In: *Nature* 431.7009, pp. 676–680 (cit. on p. 20).
- Perry, Kevin D and Hobbs, Peter V (1994). "Further evidence for particle nucleation in clear air adjacent to marine cumulus clouds". In: *Journal of Geophysical Research: Atmospheres (1984–2012)* 99.D11, pp. 22803–22818 (cit. on p. 20).
- Platt, Ulrich and Hönninger, G (2003). "The role of halogen species in the troposphere". In: *Chemosphere* 52.2, pp. 325–338 (cit. on p. 15).
- Quinn, P K and Bates, T S (2011). "The case against climate regulation via oceanic phytoplankton sulphur emissions". In: *Nature* 480.7375, pp. 51–56 (cit. on pp. 3, 11, 19–21).
- Raina, Jean-Baptiste et al. (2013). "DMSP biosynthesis by an animal and its role in coral thermal stress response". In: *Nature* 502.7473, pp. 677–680 (cit. on pp. v, 2, 23–25, 73).
- Randles, C A, Russell, L M, and Ramaswamy, V (2004). "Hygroscopic and optical properties of organic sea salt aerosol and consequences for climate forcing". In: *Geophysical Research Letters* 31.16 (cit. on p. 13).
- Rissman, T A et al. (2006). "Characterization of ambient aerosol from measurements of cloud condensation nuclei during the 2003 Atmospheric Radiation Measurement Aerosol Intensive Observational Period at the Southern Great Plains site in Oklahoma". In: *Journal of Geophysical Research* 111.D5, D05S11–20 (cit. on p. 12).
- Rogers, RR and Yau, MK (1989). *A short course of cloud physics*. Pergamon. 3rd ed. Oxford (cit. on pp. 9, 10, 13).
- Rolph, G D, Ngan, F, and Draxler, R R (2014). "Modeling the fallout from stabilized nuclear clouds using the HYSPLIT atmospheric dispersion model". In: *Journal of environmental radioactivity* 136, pp. 41–55 (cit. on p. 28).
- Rolph, Glenn D et al. (2010). "Description and Verification of the NOAA Smoke Forecasting System: The 2007 Fire Season". In: 24.2, pp. 361–378 (cit. on p. 28).
- Seinfeld, J H and Pandis, S N (2012). *Atmospheric Chemistry and Physics: From Air Pollution to Climate Change*. Wiley (cit. on pp. 7–14, 27, 43, 71, 72).
- Simpson, R M C et al. (2014). "Dimethyl sulfide: Less important than long-range transport AS a source of sulfate to the remote tropical Pacific marine boundary

BIBLIOGRAPHY

- layer”. In: *Journal of Geophysical Research D: Atmospheres* 119.14, pp. 9142–9167 (cit. on pp. 1, 31).
- Spracklen, D et al. (2003). “Development and application of a global model of aerosol processes (GLOMAP)”. In: *EGS-AGU-EUG Joint Assembly*. Vol. 1, p. 7363 (cit. on p. 43).
- Tang, Ignatius N, Tridico, AC, and Fung, KH (1997). “Thermodynamic and optical properties of sea salt aerosols”. In: *Journal of Geophysical Research: Atmospheres (1984–2012)* 102.D19, pp. 23269–23275 (cit. on p. 20).
- Thatcher, Marcus et al. (2015). “A New Approach for Coupled Regional Climate Modeling Using More than 10,000 Cores”. English. In: *Environmental Software Systems. Infrastructures, Services and Applications*. Ed. by Denzer, Ralf et al. Vol. 448. IFIP Advances in Information and Communication Technology. Springer International Publishing, pp. 599–607 (cit. on pp. 27, 39, 41).
- Todd, Jonathan D et al. (2007). “Structural and regulatory genes required to make the gas dimethyl sulfide in bacteria”. In: *Science* 315.5812, pp. 666–669 (cit. on p. 23).
- Twomey, S. (1977). *Atmospheric aerosols*. Elsevier Scientific Publishing Co., New York, NY (cit. on p. 18).
- Vairavamurthy, A, Andreae, M O, and Iverson, R L (1985). “Biosynthesis of dimethylsulfide and dimethylpropiothetin by Hymenomonas carterae in relation to sulfur source and salinity variations”. In: *Limnology and Oceanography* 30.1, pp. 59–70 (cit. on p. 17).
- Woodhouse, M T et al. (2010). “Low sensitivity of cloud condensation nuclei to changes in the sea-air flux of dimethyl-sulphide”. In: *Atmospheric Chemistry and Physics* 10.16, pp. 7545–7559 (cit. on pp. v, 3, 20, 31, 32).
- Zuidema, Paquita, Xue, Huiwen, and Feingold, Graham (2008). “Shortwave radiative impacts from aerosol effects on marine shallow cumuli”. In: *Journal of the Atmospheric Sciences* 65.6, pp. 1979–1990 (cit. on p. 20).